Universität Stuttgart

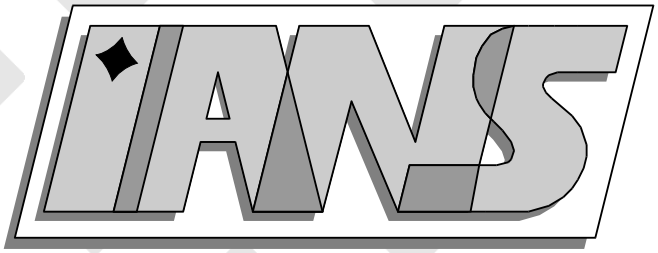

A primal-dual active set strategy for unilateral non-linear dynamic contact problems of thin-walled structures

S.Hartmann, S.Brunssen, E. Ramm, B. Wohlmuth

Berichte aus dem Institut für Angewandte Analysis und Numerische Simulation

Preprint 2006/003

Universität Stuttgart

A primal-dual active set strategy for unilateral non-linear dynamic contact problems of thin-walled structures

S.Hartmann, S.Brunssen, E. Ramm, B. Wohlmuth

Berichte aus dem Institut für Angewandte Analysis und Numerische Simulation

Preprint 2006/003

Institut für Angewandte Analysis und Numerische Simulation (IANS)
Fakultät Mathematik und Physik
Fachbereich Mathematik
Pfaffenwaldring 57
D-70 569 Stuttgart

E-Mail: ians-preprints@mathematik.uni-stuttgart.de
WWW: http://preprints.ians.uni-stuttgart.de

ISSN **1611-4176**

A primal-dual active set strategy for unilateral non-linear dynamic contact problems of thin-walled structures

S. HARTMANN, S. BRUNSSEN, E. RAMM AND B. WOHLMUTH

Abstract

The efficient modeling of 3D contact problems is still a challenge in non-linear implicit structural analysis. One part of the existing contact algorithms use penalty methods to satisfy the contact constraints, which necessitates a user defined penalty parameter. As it is well known, the choice of this additional parameter is somehow arbitrary, problem dependent and influences the accuracy of the analysis. Also contact algorithms, using standard Lagrange multipliers are well established.

We use a primal-dual active set strategy [12], based on dual Lagrange multipliers [13, 29] to handle the non-linearity of the contact conditions. This allows us to enforce the contact constraints in a weak, integral sense without any additional parameter. Due to the biorthogonality condition of the basis functions, the Lagrange multipliers can be locally eliminated. We perform a static condensation to get a reduced system for the displacements. The Lagrange multipliers, representing the contact pressure, can be easily recovered from the displacements in a variationally consistent way.

For the application to thin-walled structures we adapt a three-dimensional non-linear shell formulation, including the thickness stretch of the shell [5] to contact problems. A reparametrization of the geometric description of the shell body gives us a surface oriented shell element, which allows to apply the contact conditions directly to nodes lying on the contact surface. Shell typical locking phenomena are treated with classical concepts like EAS and ANS.

The discretization in time is done with the implicit Generalized-α Method [7] and the Generalized Energy-Momentum Method [16] to compare the development of energies within a frictionless contact description.

To conserve the total energy within the discretized frictionless contact framework, we follow an approach from Laursen and Love [19], who introduce a discrete contact velocity to update the velocity field in a post processing step.

Various examples show the good performance of the primal-dual active set strategy applied to the implicit dynamic analysis of thin-walled structures.

1 INTRODUCTION

This paper deals with the simulation of large deformation contact problems within the context of non-linear implicit structural dynamics. A great number of contact algorithms developed in the past, enforce the contact constraints at specific collocation points. Using a node-to-segment approach, the main idea is, that a specific node on the "slave side" must not penetrate the opposing "master side" segment. Although this approach is quite popular and available in numerous commercial finite element codes, the robustness of these methods is still a limitation in certain applications. So-called single pass algorithms do not satisfy the contact patch test [23], where a flat contact surface should be able to transmit a spatially constant contact pressure from one body to the other. Using low order finite elements, the unsmooth representation of the real geometry will have a significant influence on the performance of a node-to-segment approach. It will cause jumps in the contact forces, once a slave node slides off the contacting master segment. Various smoothing algorithms have been proposed to overcome these deficiencies, e.g. [24, 22, 28]. Proposed two pass algorithms indeed pass the contact path test for 2D and some 3D mesh configurations, but they suffer in turn from locking or over constraint.

Due to these drawbacks of the classical contact algorithms, the research for segment-to-segment contact strategies became quite active in recent years. Most of these new approaches use the so-called mortar method, initially introduced as a domain decomposition method by Bernardi and

co-workers [2]. Yang et al. [30] describe a contact method for two dimensional large deformation frictional sliding. Puso and Laursen [25, 26] develop a mortar segment-to-segment contact method for large deformation solid mechanics for three dimensional applications. McDevitt and Laursen [20] introduce an intermediate mortar surface to project the contact conditions between two contacting surfaces.

All formulations mentioned above use a kind of regularization technique to handle the non-linearity of the contact conditions. Popular methods in use are the penalty method and augmented Lagrangian formulation. Both methods require a user defined penalty parameter, the choice of which is problem dependent and might influence the accuracy of the analysis. Methods using standard Lagrange multipliers have the drawback that they increase the size of the system matrix and are therefore not suitable for large finite element codes.

In our formulation, we use a primal-dual active set strategy [12], which allows us to enforce the contact constraints without any additional parameter. A 2D Mortar formulation was also used by Fischer and Wriggers [8]. The success of this strategy is based on the introduction of dual Lagrange multipliers [29] to discretize the contact pressure. Following the approach described in Hüeber and Wohlmuth [13] we end up with an algebraic structure of the problem, which allows us to locally eliminate the introduced Lagrange multipliers. The contact pressure can be regarded as an external force which is dual to the contact displacement and therefore be easily recovered from the displacements in a variationally consistent way. A remarkable consequence of this strategy is the avoidance of an awkward linearization of the contact virtual work expression, which is in truth one of the most challenging parts in developing robust contact algorithms.

We present our contact formulation in the context of implicit structural dynamics, using two different time discretization schemes, the Generalized-α Method [7] and the Generalized Energy-Momentum Method [16].To end up with an energy conserving framework, we pick up an idea by Laursen and Love [19], who introduce a discrete contact velocity to update the velocity field in a post processing step. The necessary generalization of this approach according to the utilized time integration schemes, as well as the embedment into the primal-dual active set strategy is presented. Finally, we embed the algorithm to a surface oriented shell element, based on a three-dimensional 7-parameter formulation, including the thickness stretch of the shell [5].

The paper will be organized as follows. In Section 2, we will shortly describe the problem we want to analyze and introduce the notation, subsequently used in the paper. This will be followed by the spatial discretization of the contact virtual work expression, using dual Lagrange multipliers in Section 3. Section 4 deals with the description of two slightly different time discretization schemes, the Generalized-α Method and the Generalized Energy-Momentum Method. In Section 5, the active set strategy to enforce the contact constraints is presented. The spatial discretization is done with surface oriented shell elements, shortly described in Section 6. An energy conserving framework for frictionless contact is generalized according to the presented time integration schemes in Section 7. The performance of the presented strategies will be analyzed with various examples in Section 8. Some conclusions are given in Section 9.

2 PROBLEM DESCRIPTION

In this section we will briefly review the one body, rigid obstacle problem for large deformations, and introduce the notation used throughout this paper. The boundary value problem for non-linear elastodynamics is shortly presented as well as the weak form of the given problem.

2.1 One body contact with rigid obstacle

A three dimensional, large deformation one body contact problem is shown in Figure 1. The rigid obstacle is represented by the open set Ω_{obs} and its potential contact surface is denoted with Γ_{obs}. The deformable body is represented by the open sets Ω and $\overline{\Omega}$ in the reference and current configuration, respectively. We will use the notation $(\overline{\bullet})$ for all quantities corresponding to the current configuration. The surface $\partial\Omega = \Gamma$ is divided into Γ_u and Γ_σ, where displacements and

tractions are prescribed and into Γ_c, where the contact constraints will be defined. For the sake of clarity, only the contact surfaces Γ_c and $\overline{\Gamma}_c$ are shown in Figure 1.

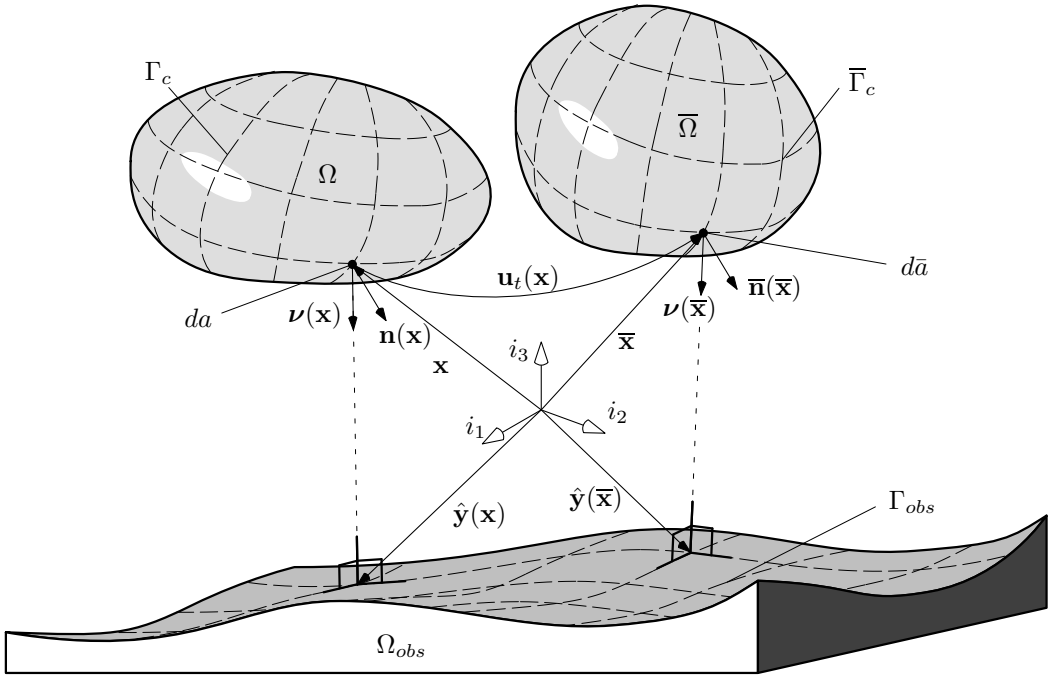

Figure 1: Notation for one body large deformation contact problem

Considering a point $\mathbf{x}$ on the contact surface of the deformable body, we define a corresponding point $\hat{\mathbf{y}}(\mathbf{x})$ on Γ_{obs} as a result of the closest point projection given by

$$\hat{\mathbf{y}}(\mathbf{x}) = \arg \min_{\mathbf{y} \in \Gamma_{obs}} ||\mathbf{x} - \mathbf{y}||. \tag{1}$$

The motion of the deformable body from the reference to the current configuration at time t is given by

$$\overline{\mathbf{x}} = \mathbf{x} + \mathbf{u}_t. \tag{2}$$

We define the scalar valued gap function as

$$g(\mathbf{x}, t) = g(\overline{\mathbf{x}}) = -\boldsymbol{\nu}(\overline{\mathbf{x}}) \cdot (\overline{\mathbf{x}} - \hat{\mathbf{y}}(\overline{\mathbf{x}})) \tag{3}$$

where $\boldsymbol{\nu}$ denotes the unit normal on Γ_{obs} at $\hat{\mathbf{y}}$ pointing into Ω_{obs}. The sign of this gap function will define whether a material point on $\overline{\Gamma}_c$ will come into contact with the rigid obstacle or not. A positive value of $g(\mathbf{x}, t)$ indicates that there is no contact, whereas a negative value describes an interpenetration, which is prohibited, such that the kinematic constraint reads

$$g(\mathbf{x}, t) \geq 0. \tag{4}$$

The contact tractions w.r.t. the reference configuration $\mathbf{t}$ and the contact tractions w.r.t. the actual configuration $\overline{\mathbf{t}}$ at a specific point $\mathbf{x} \in \Gamma_c$ are defined as

$$\begin{aligned} \mathbf{t} &= \mathbf{P}(\mathbf{x}) \cdot \mathbf{n}(\mathbf{x}) \\ \overline{\mathbf{t}} &= \boldsymbol{\sigma}(\overline{\mathbf{x}}, t) \cdot \overline{\mathbf{n}}(\overline{\mathbf{x}}), \end{aligned}$$

where $\mathbf{n}$ and $\overline{\mathbf{n}}$ are the outward unit normal on Ω and $\overline{\Omega}$, respectively. Due to the definition of the first Piola Kirchhoff stress tensor $\mathbf{P}$, the Cauchy stress tensor $\boldsymbol{\sigma}$ and Nanson's formula (1878), we find that

$$\mathbf{t} = \frac{d\bar{a}}{da} \cdot \overline{\mathbf{t}} \tag{5}$$

where $da, d\bar{a}$ are the differential areas in the reference and actual configuration, respectively. From this we can see that the difference between the actual contact tractions and the reference contact tractions is only the change in the area resulting from the deformation $\frac{d\bar{a}}{da}$ which is a positive number. Since each of the following considerations involving the contact tractions will only depend on their sign, we can work with the contact tractions measured in the reference configuration. This traction vector can be decomposed into a scalar normal part t_ν and a vector valued tangential part $\mathbf{t}_\tau$ as

$$\mathbf{t} = t_\nu \cdot \boldsymbol{\nu} - \mathbf{t}_\tau, \qquad t_\nu = \mathbf{t} \cdot \boldsymbol{\nu}. \tag{6}$$

As we will restrict ourselves to frictionless contact, the tangential part of the contact traction vanishes, and we can express the contact constraints in form of the classical Karush-Kuhn-Tucker conditions:

$$\begin{aligned} t_\nu &\leq 0, \\ g(\mathbf{x}, t) &\geq 0, \\ t_\nu \; g(\mathbf{x}, t) &= 0. \end{aligned} \tag{7}$$

Equation $(8)_1$ requires that the normal contact forces t_ν have to be compressive, as we do not consider adhesion, Equation $(8)_2$ is the geometric impenetrability condition and Equation $(8)_3$ ensures that contact forces have non-zero values only when the gap is closed ($g(\mathbf{x}, t) = 0$), thus contact exists.

2.2 Boundary value problem of non-linear elastodynamics

In the context of large deformation, non-linear elastodynamics, we have to consider the following boundary value problem

$$\begin{aligned} \rho\ddot{\mathbf{u}} &= div\ (\mathbf{F} \cdot \mathbf{S}) + \rho\mathbf{b} && \text{in} \quad \Omega, \\ \mathbf{u} &= \hat{\mathbf{u}} && \text{on} \quad \Gamma_u, \\ \mathbf{t} &= \hat{\mathbf{t}} && \text{on} \quad \Gamma_\sigma, \end{aligned} \tag{8}$$

where $\mathbf{F}$, $\mathbf{S}$ and $\mathbf{b}$ are the material deformation gradient, the second Piola-Kirchhoff stress tensor and the volume forces on Ω, respectively. Appropriate boundary conditions are given by the prescribed displacements $\hat{\mathbf{u}}$ and tractions $\hat{\mathbf{t}}$, acting on the correlated boundaries Γ_u and Γ_σ. The second Piola-Kirchhoff stress tensor is given via an appropriate constitutive relation, e.g. for St. Venant-Kirchhoff material:

$$\mathbf{S} = \mathbf{C} : \mathbf{E} \tag{9}$$

with $\mathbf{C}$ being the constitutive tensor and $\mathbf{E}$ representing the Green-Lagrange strain tensor defined as

$$\mathbf{E} = \frac{1}{2}\left(\mathbf{F}^\top \cdot \mathbf{F} - \mathbf{I}\right). \tag{10}$$

2.3 Weak form

We will now introduce the weak form of this problem as the mathematical basis for the finite element method. Using appropriate spaces for the displacements $\mathbf{u}$ and the virtual displacements $\delta\mathbf{u}$ the virtual work principle for the one body contact problem in large deformation, non-linear elastodynamics can be written as

$$\delta\Pi(\mathbf{u}, \delta\mathbf{u}) = \delta\Pi^{int,ext}(\mathbf{u}, \delta\mathbf{u}) + \delta\Pi^{c}(\mathbf{u}^c, \delta\mathbf{u}^c) = 0. \tag{11}$$

where the displacements on Γ_c are denoted by $\mathbf{u}^c$. The first expression represents the usual virtual work statement without contact, given as

$$\delta\Pi^{int,ext}(\mathbf{u}, \delta\mathbf{u}) = \int_\Omega \left[\rho\ddot{\mathbf{u}} \cdot \delta\mathbf{u} + \delta\mathbf{E} : \mathbf{S} - \rho\mathbf{b} \cdot \delta\mathbf{u}\right] \, d\Omega - \int_{\Gamma_\sigma} \hat{\mathbf{t}} \cdot \delta\mathbf{u} \, d\Gamma_\sigma, \tag{12}$$

whereas the second part denotes the virtual work associated with the contact tractions, defined as

$$\delta\Pi^c(\mathbf{u}^c, \delta\mathbf{u}^c) = -\int_{\Gamma_c} \mathbf{t} \cdot \delta\mathbf{u}^c \; d\Gamma_c, \tag{13}$$

We introduce a Lagrange multiplier $\boldsymbol{\lambda}$, [14] representing the negative contact tractions ($\boldsymbol{\lambda} = -\mathbf{t}$). The idea is to interpret the contact traction as a given external surface traction, so that we do not treat it as an additional unknown.

3 SPATIAL DISCRETIZATION OF CONTACT VIRTUAL WORK

To solve the aforementioned problem (8) and (11), we discretize the deformable body Ω using finite elements. Without going into detail about the specific element formulation (see Section 6), we use standard isoparametric shape functions in the three dimensional setting. The spatial configuration of the contact surface mesh inherits its triangulation from the three-dimensional discretization and can be parameterized in the following way

$$\mathbf{x} \approx \mathbf{x}_h = \sum_{i=1}^{nc} N_i \; \mathbf{x}_i, \qquad \text{where} \qquad \mathbf{x}, \mathbf{x}_h : \Gamma_c \to \mathbb{R}^3, \quad \mathbf{x}_i \in \mathbb{R}^3. \tag{14}$$

Here nc is the number of nodes defined on the surface mesh of Γ_c, $N_i : \Gamma_c \to \mathbb{R}$ are the classical nodal shape functions and $\mathbf{x}_i$ are the nodal coordinates. By $\boldsymbol{\lambda}_i \in \mathbb{R}^3$ we denote the vector of contact tractions at the node $i \in \Gamma_c$. We introduce the discrete Lagrange multiplier basis functions $M_i : \Gamma_c \to \mathbb{R}$

$$\boldsymbol{\lambda} \approx \boldsymbol{\lambda}_h = \sum_{i=1}^{nc} M_i \; \boldsymbol{\lambda}_i \tag{15}$$

such that the so-called biorthogonality condition of the basis functions

$$\int_{\Gamma_c} M_i N_j \; d\Gamma_c = \delta_{ij} \int_{\Gamma_c} N_j \; d\Gamma_c \tag{16}$$

is satisfied. The algorithmic advantage of this choice will be explained in Section 5.2. In case of quadrilateral elements on Γ_c with a constant functional determinant, the ansatz-functions for the Lagrange multipliers in the isoparametric space can be specified a priori. In Figure 2a and 2c, the standard bi-linear shape functions $\hat{N}_1, \ldots, \hat{N}_4 : [-1, 1]^2 \to \mathbb{R}$

$$\begin{aligned}
\hat{N}_1 &= \frac{1}{4}(1-\xi)(1-\eta) \qquad \text{(shown)} \\
\hat{N}_2 &= \frac{1}{4}(1+\xi)(1-\eta) \\
\hat{N}_3 &= \frac{1}{4}(1+\xi)(1+\eta) \\
\hat{N}_4 &= \frac{1}{4}(1-\xi)(1+\eta)
\end{aligned}$$

and the corresponding dual basis functions for parallelogram shaped elements are given in the isoparametric space. For any arbitrary shaped elements, the ansatz-functions for the discretized dual Lagrange multipliers have to be constructed [9]. Without detailing the theory, we want to present the necessary steps to derive the appropriate discretized Lagrange multipliers, fulfilling the biorthogonality condition with the standard bi-linear shape functions.

3.1 Discrete dual Lagrange multipliers for arbitrary shaped elements

Let us define with T and $\hat{T} = [-1,1]^2$ a 4-noded element on the contact boundary Γ_c, given in the physical and the isoparametric space, respectively. Furthermore we denote by $\mathbf{F}_T : \hat{T} \to T \subset \mathbb{R}^3$ the element mapping such that $\hat{N}_i = N_i \circ \mathbf{F}_T$. Our aim is now the biorthogonality (16) element-wise on $T \subset \Gamma_c$:

$$\int_T M_i N_j \; dT = \delta_{ij} \int_T N_j \; dT. \tag{17}$$

Therefore we construct the ansatz-functions for the Lagrange multipliers in the following way:

$$\hat{M}_i = \sum_k a_{ik} \hat{N}_k, \quad \text{with} \quad \mathbf{A}_T = a_{ij} = \mathbf{D}_T \; \mathbf{M}_T^{-1} \quad \in \mathbb{R}^{4\times 4} \tag{18}$$

and therein $\mathbf{D}_T = \delta_{ij} \int_T N_j dT$ the desired diagonal matrix and with $\mathbf{M}_T = \int_T N_i N_j dT$ the element matrix, which is due to its analogy also called mass matrix. Then we verify:

$$\begin{aligned}
\int_T M_i N_j dT &= \int_{\hat{T}} J \hat{M}_i \hat{N}_j d\hat{T} \\
&= \int_{\hat{T}} J \sum_k a_{ik} \hat{N}_k \hat{N}_j d\hat{T} \\
&= \sum_k a_{ik} \int_{\hat{T}} J \hat{N}_k \hat{N}_j d\hat{T} \\
&= \sum_k a_{ik} [\mathbf{M}_T]_{kj} \\
&= [\mathbf{A}_T \mathbf{M}_T]_{ij} = [\mathbf{D}_T]_{ij}
\end{aligned} \tag{19}$$

Herein $J = \det(\mathbf{F}_T)$ is the Jacobian determinant of an element T. To further illustrate this procedure we will exemplarily calculate one discrete ansatz-function for the dual Lagrange multipliers for two different element shapes. The first one having a regular shape, resulting in a constant Jacobian determinant $J = const$, and the second one being of arbitrary shape with $J \neq const$.

Undistorted Element:

$$(\mathbf{x}, \mathbf{y}, \mathbf{z})^\top = \begin{bmatrix} 0 & 2 & 2 & 0 \\ 0 & 0 & 2 & 2 \\ 0 & 0 & 0 & 0 \end{bmatrix}$$

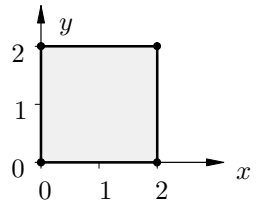

The resulting transformation matrix is:

$$\mathbf{A}_T = \begin{bmatrix} 4 & -2 & 1 & -2 \\ -2 & 4 & -2 & 1 \\ 1 & -2 & 4 & -2 \\ -2 & 1 & -2 & 4 \end{bmatrix}$$

So we can compute for example the discretized Lagrange multiplier $\hat{M}_1$ in the isoparametric space $[\xi, \eta] \in [-1,1]^2$ from Equation (18):

$$\begin{aligned}
\hat{M}_1 &= 4\hat{N}_1 - 2\hat{N}_2 + 1\hat{N}_3 - 2\hat{N}_4 \\
&= \frac{1}{4}(1-3\xi)(1-3\eta)
\end{aligned}$$

$$\hat{M}_1(-1,-1) = 4 \quad \hat{M}_1(1,-1) = -2 \quad \hat{M}_1(1,1) = 1 \quad \hat{M}_1(-1,1) = -2$$

which is always the case for constant J.

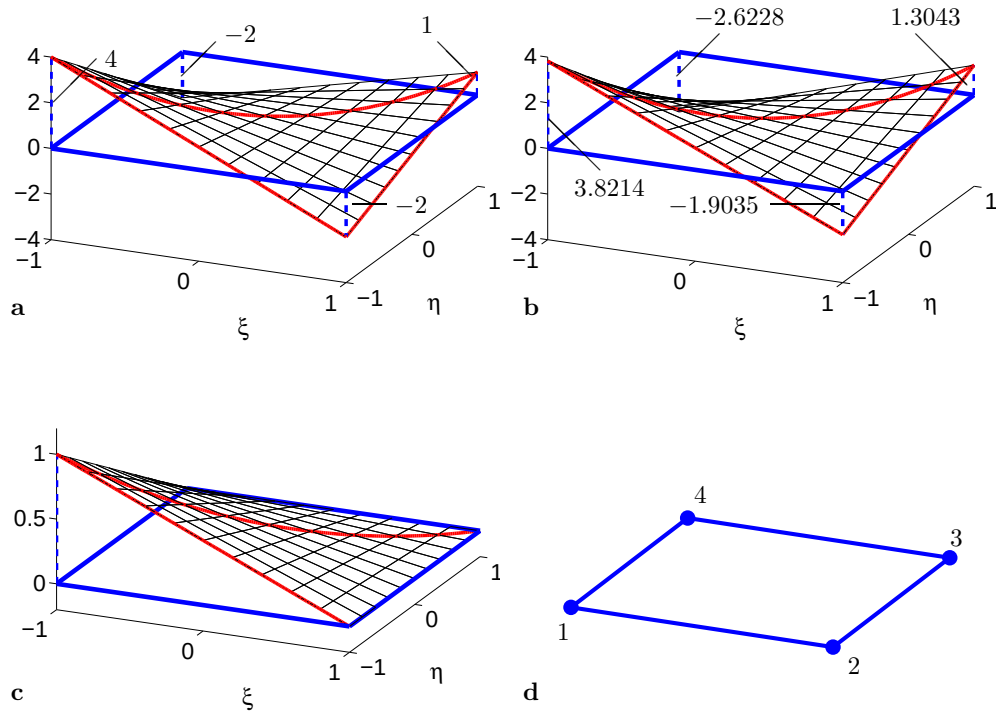

Figure 2: Plot of $\hat{M}_1$ for the undistorted (a), for the distorted (b) element, plot of the shape function $\hat{N}_1$ (c) and plot of the ordering of the shape functions $\hat{N}_1, \ldots, \hat{N}_4$ (d)

Distorted Element:

$$(\mathbf{x}, \mathbf{y}, \mathbf{z})^\top = \begin{bmatrix} 1 & 2 & 1.8 & 1.5 \\ 1 & 1.3 & 2.1 & 2 \\ 0 & 0 & 0 & 0 \end{bmatrix}$$

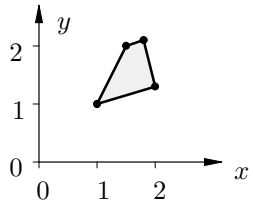

The resulting transformation matrix is:

$$\mathbf{A}_T = \begin{bmatrix} 3.8214 & -1.9035 & 1.3043 & -2.6228 \\ -1.9132 & 3.8118 & -2.6075 & 1.3109 \\ 0.9116 & -1.8133 & 4.6024 & -2.3161 \\ -1.8199 & 0.9050 & -2.2992 & 4.6280 \end{bmatrix}$$

Again, we can compute the discretized Lagrange multiplier $\hat{M}_1$:

$$\hat{M}_1 = 3.8214\hat{N}_1 - 1.9035\hat{N}_2 + 1.3043\hat{N}_3 - 2.6228\hat{N}_4$$

$$\hat{M}_1(-1,-1) = 3.8214 \quad \hat{M}_1(1,-1) = -1.9035 \quad \hat{M}_1(1,1) = 1.3043 \quad \hat{M}_1(-1,1) = -2.6228$$

In Figure 2a and 2b the ansatz-functions $\hat{M}_1$ is shown for the undistorted and the distorted element, respectively. The general structure of the interpolation functions remains the same, but the basis values at the nodes of the elements vary.

3.2 Discrete form of contact virtual work

Using the above mentioned interpolations for the displacement and contact pressure field, we can approximate the contact virtual work expression (13) in the discrete form

$$\begin{aligned} \delta\Pi^c(\mathbf{u}^c, \delta\mathbf{u}^c) \approx \delta\Pi_h^c(\mathbf{u}_h^c, \delta\mathbf{u}_h^c) &= \int_{\Gamma_c} \boldsymbol{\lambda}_h \cdot \delta\mathbf{u}_h^c \; d\Gamma_c \\ &= \int_{\Gamma_c} \sum_{i=1}^{nc} M_i \boldsymbol{\lambda}_i \cdot \sum_{j=1}^{nc} N_j \delta\mathbf{u}_j \; d\Gamma_c \\ &= \sum_{i=1}^{nc}\sum_{j=1}^{nc} \delta\mathbf{u}_j^\top \int_{\Gamma_c} M_i N_j \; d\Gamma_c \; \boldsymbol{\lambda}_i. \end{aligned} \tag{20}$$

By $\delta\mathbf{u}_i \in \mathbb{R}^3$ we denote the vector of virtual displacements at the node $i \in \Gamma_c$. Due to the biorthogonality condition (16), this representation simplifies drastically. We define the diagonal Matrix $\mathbf{D} \in \mathbb{R}^{3nc\times 3nc}$, which block entries are given by

$$\mathbf{D}[i,i] := \int_{\Gamma_c} N_i \; d\Gamma_c \; \mathbf{I}_3, \qquad \text{for} \qquad i = 1, \ldots, nc, \tag{21}$$

to express the contact virtual work in a compact vector-matrix notation. Herein $\mathbf{I}_3$ denotes the identity matrix in $\mathbb{R}^{3\times 3}$. In the following, we will identify the functions $\delta\mathbf{u}_h^c$ and $\boldsymbol{\lambda}_h$ with the vector of all nodal values. The contact virtual work expression now reads

$$\delta\Pi_h^c = (\delta\mathbf{u}^c)^\top \; \mathbf{D} \; \boldsymbol{\lambda}, \tag{22}$$

where $\boldsymbol{\lambda}$ and $\delta\mathbf{u}^c$ are vectors of length $3nc$, containing all the discrete nodal values of the Lagrange multiplier and the virtual displacements on the contact surface nodes.
In order to get a compact algebraic expression of the whole problem described in Section 2, we divide all vertices on Ω into a subset $\mathcal{S}$, the set of potential contact nodes, containing all nodes on Γ_c and $\mathcal{N}$ for the remaining vertices. As the Lagrange multipliers represent the contact pressure on Γ_c, the diagonal matrix $\mathbf{D}$ has to be expanded to give a matrix expression for the contact tractions depending on all degrees of freedom of the discretized problem. Therefore we introduce the matrix $\tilde{\mathbf{D}} \in \mathbb{R}^{3nd\times 3nc}$, having the form $\tilde{\mathbf{D}} = (\mathbf{0}, \mathbf{D})^\top$, where nd is the total number of discrete nodes defined in Ω.

3.3 Semidiscrete initial value problem

Starting from the weak form (11) of the non-linear, dynamic contact problem, the semidiscrete equation of motion is derived introducing the spatial discretization via finite elements:

$$\mathbf{M}\ddot{\mathbf{u}} + \mathbf{C}\dot{\mathbf{u}} + \mathbf{F}^{int}(\mathbf{u}) + \mathbf{F}^c = \mathbf{F}^{ext}. \tag{23}$$

Herein, $\mathbf{M}$ represents the mass matrix, $\mathbf{C}$ the viscous damping matrix, $\mathbf{F}^{int}(\mathbf{u})$ the deformation dependent internal forces, $\mathbf{F}^c$ the contact forces, $\mathbf{F}^{ext}$ the external forces, $\mathbf{u}$ is the vector of the structural displacements, $\dot{\mathbf{u}}$ are the velocities, and $\ddot{\mathbf{u}}$ are the accelerations. Consequently the inertia forces and damping forces are given by $\mathbf{M}\ddot{\mathbf{u}}$ and $\mathbf{C}\dot{\mathbf{u}}$, respectively. Due to the lack of information about the damping mechanisms in structures, the damping matrix is assumed to be a linear combination of the mass matrix and the elastic stiffness matrix $\mathbf{K}^e(\mathbf{u} = \mathbf{0})$, called proportional or Rayleigh damping.

If we order the vectors of nodal unknown displacements $\mathbf{u} = (\mathbf{u}_\mathcal{N}, \mathbf{u}_\mathcal{S})^\top$ and Lagrange multipliers $\boldsymbol{\lambda}$ according to the two subsets introduced before, the contact forces can be expressed as (see Equation 22)

$$\mathbf{F}^c = \tilde{\mathbf{D}} \; \boldsymbol{\lambda}. \tag{24}$$

It is worth noting that the determination of the entries of $\tilde{\mathbf{D}}$ can be performed in the reference configuration. This will have the favorable consequence that the weighting factors have to be calculated only once, thus no linearization is necessary for $\tilde{\mathbf{D}}$.

4 TIME DISCRETIZATION

To integrate the semidiscrete problem (23), the time interval of interest $[0, T]$ is subdivided into typical time intervals $[t_n, t_{n+1}]$ with the corresponding time step $\Delta t = t_{n+1} - t_n$. Given the state variables $\mathbf{u}_n$, $\dot{\mathbf{u}}_n$ and $\ddot{\mathbf{u}}_n$ at time t_n, we solve Equation (23) in an implicit way, to obtain the solution of the state variables $\mathbf{u}_{n+1}$, $\dot{\mathbf{u}}_{n+1}$ and $\ddot{\mathbf{u}}_{n+1}$ at the end of each time step. To reduce the set of unknown variables to the displacements $\mathbf{u}_{n+1}$, the classical Newmark approximations [21] are used.

$$\begin{aligned} \mathbf{u}_{n+1}(\ddot{\mathbf{u}}_{n+1}) &= \mathbf{u}_n + \Delta t\ \dot{\mathbf{u}}_n + \tfrac{1-2\beta}{2}\Delta t^2\ \ddot{\mathbf{u}}_n + \beta \Delta t^2\ \ddot{\mathbf{u}}_{n+1} \\ \dot{\mathbf{u}}_{n+1}(\ddot{\mathbf{u}}_{n+1}) &= \dot{\mathbf{u}}_n + (1-\gamma)\Delta t\ \ddot{\mathbf{u}}_n + \gamma \Delta t\ \ddot{\mathbf{u}}_{n+1} \end{aligned} \tag{25}$$

Equivalently we rewrite the velocities and accelerations in terms of the displacement at time t_{n+1}.

$$\begin{aligned} \dot{\mathbf{u}}_{n+1}(\mathbf{u}_{n+1}) &= \tfrac{\gamma}{\beta\Delta t}(\mathbf{u}_{n+1} - \mathbf{u}_n) - \left(\tfrac{\gamma}{\beta} - 1\right)\dot{\mathbf{u}}_n - \left(\tfrac{\gamma}{2\beta} - 1\right)\Delta t\ \ddot{\mathbf{u}}_n \\ \ddot{\mathbf{u}}_{n+1}(\mathbf{u}_{n+1}) &= \tfrac{1}{\beta\Delta t^2}(\mathbf{u}_{n+1} - \mathbf{u}_n) - \tfrac{1}{\beta\Delta t}\dot{\mathbf{u}}_n - \left(\tfrac{1}{2\beta} - 1\right)\ddot{\mathbf{u}}_n \end{aligned} \tag{26}$$

In the following, we will describe two slightly different time integration schemes, both based on the given Newmark scheme. The Generalized-α Method (Gen-α), originally proposed for linear dynamical systems by Chung and Hulbert [7] and the Generalized Energy-Momentum Method (GEMM) developed by Kuhl and Crisfield [15] for trusses and later adapted for non-linear shell dynamics by Kuhl and Ramm [16]. Both methods apply the semidiscrete equation of motion (23) at a generalized mid-point configuration

$$\mathbf{M}\ \ddot{\mathbf{u}}_{n+1-\alpha_m} + \mathbf{C}\ \dot{\mathbf{u}}_{n+1-\alpha_f} + \mathbf{F}^{int}(\mathbf{u}_{n+1-\alpha_f}) + \mathbf{F}^{c}_{n+1-\alpha_f} = \mathbf{F}^{ext}_{n+1-\alpha_f}, \tag{27}$$

described via two shift parameters α_m and α_f. Herein, the subscripts denote the time discrete combinations of the accelerations, velocities, displacements as well as the internal, the contact and the external forces.

$$\begin{aligned} \ddot{\mathbf{u}}_{n+1-\alpha_m} &= (1-\alpha_m)\ddot{\mathbf{u}}_{n+1} + \alpha_m \ddot{\mathbf{u}}_n, \\ \dot{\mathbf{u}}_{n+1-\alpha_f} &= (1-\alpha_f)\dot{\mathbf{u}}_{n+1} + \alpha_f \dot{\mathbf{u}}_n, \\ \mathbf{u}_{n+1-\alpha_f} &= (1-\alpha_f)\mathbf{u}_{n+1} + \alpha_f \mathbf{u}_n, \\ \mathbf{F}^{int}(\mathbf{u}_{n+1-\alpha_f}) &= \begin{cases} (1-\alpha_f)\mathbf{F}^{int}_{n+1} + \alpha_f \mathbf{F}^{int}_{n}, & \text{for Gen-}\alpha \\ \mathbf{F}^{int}\left((1-\alpha_f)\mathbf{u}_{n+1} + \alpha_f \mathbf{u}_n\right), & \text{for GEMM} \end{cases} \\ \mathbf{F}^{ext}_{n+1-\alpha_f} &= (1-\alpha_f)\mathbf{F}^{ext}_{n+1} + \alpha_f \mathbf{F}^{ext}_{n}. \end{aligned} \tag{28}$$

The crucial difference between the Generalized-α Method and the Generalized Energy-Momentum Method is the calculation of the internal forces at the generalized mid-point configuration. In the Generalized-α Method, the internal forces are approximated using the general trapezoidal rule, whereas in the General Energy-Momentum Method the internal forces are calculated at the mid-point configuration. This is essential for this method and will have significant influence on the derivation of the deformation dependent algorithmic tangential stiffness matrix, which will be discussed separately, when describing the surface oriented shell element in Section 6. According to Equation (24) the contribution of the contact forces in Equation (27) can be expressed as

$$\mathbf{F}^{c}_{n+1-\alpha_f} = \tilde{\mathbf{D}}\ \boldsymbol{\lambda}_{n+1-\alpha_f}. \tag{29}$$

Combining the approximations of the velocities and accelerations (26) and (28) with the equation of motion (27) together with (29) yields the effective structural equation, being non-linear in the unknown displacements $\mathbf{u}_{n+1}$

$$\begin{aligned} \mathbf{G}(\mathbf{u}_{n+1}) \equiv\ & \mathbf{F}^{int}(\mathbf{u}_{n+1-\alpha_f}(\mathbf{u}_{n+1})) + \frac{1-\alpha_m}{\beta\Delta t^2}\mathbf{M}\ \mathbf{u}_{n+1} + \frac{(1-\alpha_f)\gamma}{\beta\Delta t}\mathbf{C}\ \mathbf{u}_{n+1} - \\ & \mathbf{h}(\mathbf{u}_n, \dot{\mathbf{u}}_n, \ddot{\mathbf{u}}_n) + \tilde{\mathbf{D}}\ \boldsymbol{\lambda}_{n+1-\alpha_f} - \mathbf{F}^{ext}_{n+1-\alpha_f} = \mathbf{0}, \end{aligned} \tag{30}$$

where $\mathbf{h}(\mathbf{u}_n, \dot{\mathbf{u}}_n, \ddot{\mathbf{u}}_n)$ is a history term, only dependent on the given state variables at time t_n.

$$\begin{aligned}\mathbf{h}(\mathbf{u}_n, \dot{\mathbf{u}}_n, \ddot{\mathbf{u}}_n) &= \mathbf{M}\left[\frac{1-\alpha_m}{\beta\Delta t^2}\mathbf{u}_n + \frac{1-\alpha_m}{\beta\Delta t}\dot{\mathbf{u}}_n + \frac{1-\alpha_m-2\beta}{2\beta}\ddot{\mathbf{u}}_n\right] + \\ &\quad \mathbf{C}\left[\frac{(1-\alpha_f)\gamma}{\beta\Delta t}\mathbf{u}_n + \frac{(1-\alpha_f)\gamma-\beta}{\beta}\dot{\mathbf{u}}_n + \frac{(\gamma-2\beta)(1-\alpha_f)}{2\beta}\Delta t\ddot{\mathbf{u}}_n\right] \quad (31)\end{aligned}$$

4.1 Linearization and iterative solution strategy

The non-linearity of the effective structural equation, needs an iterative solution. Therefore Equation (30) is linearized

$$\mathbf{G}\left(\mathbf{u}_{n+1}^{k+1}\right) \approx \mathbf{G}\left(\mathbf{u}_{n+1}^{k}\right) + \frac{\partial \mathbf{G}\left(\mathbf{u}_{n+1}^{k}\right)}{\partial \mathbf{u}_{n+1}}\Delta\mathbf{u} = \mathbf{0}, \quad (32)$$

with

$$\Delta\mathbf{u} = \mathbf{u}_{n+1}^{k+1} - \mathbf{u}_{n+1}^{k} \quad (33)$$

and the Newton-Raphson iteration technique is applied. This leads to the effective iterative structural equation

$$\mathbf{K}_{eff}^{k}\Delta\mathbf{u} = -\mathbf{G}(\mathbf{u}_{n+1}^{k}), \quad (34)$$

where $\mathbf{K}_{eff}^{k}$ is the effective algorithmic tangential stiffness matrix

$$\mathbf{K}_{eff}^{k} = \frac{\partial \mathbf{F}^{int}(\mathbf{u}_{n+1-\alpha_f}(\mathbf{u}_{n+1}))}{\partial \mathbf{u}_{n+1}} + \frac{1-\alpha_m}{\beta\Delta t^2}\mathbf{M} + \frac{(1-\alpha_f)\gamma}{\beta\Delta t}\mathbf{C}, \quad (35)$$

and $\mathbf{G}(\mathbf{u}_{n+1}^{k})$ are the out-of-balance forces at iteration step k. We now sort all these matrices according to our definition of subset $\mathcal{N}$ and $\mathcal{S}$ and move the contact term $(\tilde{\mathbf{D}}\ \boldsymbol{\lambda}_{n+1-\alpha_f})$ to the left hand side. With $\tilde{\mathbf{D}} = (\mathbf{0}, \mathbf{D})^\top$, we arrive at the following incremental representation of the effective structural Equation (30)

$$\begin{bmatrix} \mathbf{K}_{eff}^{\mathcal{NN}} & \mathbf{K}_{eff}^{\mathcal{NS}} & \mathbf{0} \\ \mathbf{K}_{eff}^{\mathcal{SN}} & \mathbf{K}_{eff}^{\mathcal{SS}} & \mathbf{D} \end{bmatrix}^k \begin{bmatrix} \Delta\mathbf{u}_{\mathcal{N}} \\ \Delta\mathbf{u}_{\mathcal{S}} \\ \boldsymbol{\lambda}_{n+1-\alpha_f} \end{bmatrix} = - \begin{bmatrix} \widehat{\mathbf{G}}_{\mathcal{N}}(\mathbf{u}_{n+1}^{k}) \\ \widehat{\mathbf{G}}_{\mathcal{S}}(\mathbf{u}_{n+1}^{k}) \end{bmatrix}, \quad (36)$$

with

$$\begin{aligned}\widehat{\mathbf{G}}(\mathbf{u}_{n+1}^{k}) &= \mathbf{F}^{int}(\mathbf{u}_{n+1-\alpha_f}(\mathbf{u}_{n+1}^{k})) + \frac{1-\alpha_m}{\beta\Delta t^2}\mathbf{M}\ \mathbf{u}_{n+1}^{k} + \frac{(1-\alpha_f)\gamma}{\beta\Delta t}\mathbf{C}\ \mathbf{u}_{n+1}^{k} - \\ &\quad \mathbf{h}(\mathbf{u}_n, \dot{\mathbf{u}}_n, \ddot{\mathbf{u}}_n) - \mathbf{F}_{n+1-\alpha_f}^{ext}. \quad (37)\end{aligned}$$

5 ACTIVE SET STRATEGY

5.1 Weak impenetrability condition

The main difficulty in solving contact problems is the fact that the effective structural Equation (36), derived in the last section, is constrained by the KKT conditions given in Equation (8). In an incremental setting we may rewrite the impenetrability condition (4) in the following way (see also Figure 3)

$$\Delta\mathbf{u} \cdot \boldsymbol{\nu}_{n+1}^{k} \leq g(\mathbf{x}_{n+1}^{k}, t_{n+1}), \qquad \Delta\mathbf{u}, \boldsymbol{\nu}_{n+1}^{k}, \mathbf{x}_{n+1}^{k} : \Gamma_c \to \mathbb{R}^3. \quad (38)$$

Now, this strong and point-wise constraint is replaced by a weaker integral condition

$$\int_{\Gamma_c} (\Delta\mathbf{u} \cdot \boldsymbol{\nu}_{n+1}^{k})\ v^*\ d\Gamma_c \leq \int_{\Gamma_c} g(\mathbf{x}_{n+1}^{k}, t_{n+1})\ v^*\ d\Gamma_c, \quad (39)$$

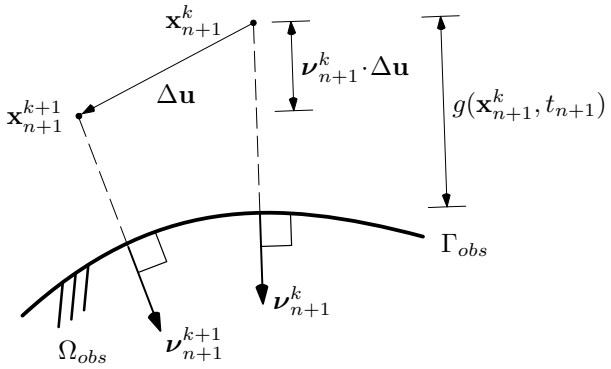

Figure 3: Impenetrability condition formulated in terms of incremental Newton scheme

where the test function $v^* : \Gamma_c \to \mathbb{R}$ will be discretized, using again the discrete dual Lagrange multiplier spaces

$$v^* \approx v_h^* = \sum_{i=1}^{nc} M_i \; v_i^*. \tag{40}$$

If we insert now the discrete approximation of the displacement increments, together with the discrete test function v_h^*, Equation (39) can be rewritten as

$$\sum_{i=1}^{nc} \sum_{j=1}^{nc} v_i^* \int_{\Gamma_c} M_i N_j \; d\Gamma_c \; (\Delta\mathbf{u}_j \cdot \boldsymbol{\nu}_{n+1,j}^k) \leq \sum_{i=1}^{nc} v_i^* \int_{\Gamma_c} g(\mathbf{x}_{n+1}^k, t_{n+1}) \; M_i \; d\Gamma_c, \tag{41}$$

where $g(\mathbf{x}_{n+1}^k, t_{n+1})$ is a suitable approximation of g, which means that the real gap along the contact surface has to be identified in a proper manner. This could be done, by evaluating the gap at intermediate points on the contact boundary and interpolating these values with some kind of interpolation functions. With the definition for the diagonal matrix $\mathbf{D}$ from Equation (21) and the biorthogonality property (16), the weak non-penetrability condition yields the compact vector matrix form (42). In addition, we collect all the vectors $\Delta\mathbf{u}_i$ and $\boldsymbol{\nu}_{n+1,i}^k$ in the vectors $\Delta\mathbf{d} \in \mathbb{R}^{3nc}$ and $\boldsymbol{n}_{n+1}^k \in \mathbb{R}^{3nc}$.

$$\left(\boldsymbol{n}_{n+1}^k\right)^\top \mathbf{D} \; \Delta\mathbf{d} \leq \mathbf{g}_{n+1}^k \in \mathbb{R}^{nc} \tag{42}$$

Herein $\mathbf{g}_{n+1}^k$ represents the vector of weighted nodal gaps, evaluated at the kth iteration step within the time interval $[t_n, t_{n+1}]$. We note that for the computation of this vector the explicit knowledge of the dual Lagrange multipliers is needed. Due to the fact that $\mathbf{D}$ is a diagonal matrix, the multi-dimensional inequality condition from Equation (42) can be cut down to a set of scalar inequality expressions for each node on the subset $\mathcal{S}$ as

$$\Delta u_{\nu,i} := \left(\boldsymbol{\nu}_{n+1,i}^k\right)^\top \mathbf{D}[i,i] \; \Delta\mathbf{u}_i \leq g_{n+1,i}^k, \qquad i \in \mathcal{S}, \tag{43}$$

where $\Delta u_{\nu,i}$ denotes the scalar residual displacement of a node $i \in \mathcal{S}$ in direction of the unit outward normal $\boldsymbol{\nu}_{n+1,i}^k \in \mathbb{R}^3$ weighted with the appropriate entry of the diagonal matrix $\mathbf{D}[i,i] \in \mathbb{R}^{3\times3}$. The right hand side of Equation (43) can be interpreted as a weighted nodal gap. Splitting the discrete Lagrange multiplier $\boldsymbol{\lambda}_i \in \mathbb{R}^3$ at the vertex $i \in \mathcal{S}$ into its normal and tangential part according to (6)

$$\boldsymbol{\lambda}_i = \lambda_{\nu,i} \cdot \boldsymbol{\nu}_i - \boldsymbol{\lambda}_{\tau,i}, \tag{44}$$

we can summarize our incremental problem.

Solve the incremental effective structural Equation (36) considering the following discrete constraints

$$\begin{aligned} \Delta u_{\nu,i} &\leq g_{n+1,i}^k, \qquad \lambda_{\nu,i} \geq 0, \qquad \lambda_{\nu,i}(\Delta u_{\nu,i} - g_{n+1,i}^k) = 0, \\ \boldsymbol{\lambda}_{\tau,i} &= \mathbf{0} \end{aligned} \tag{45}$$

for all vertices $i \in \mathcal{S}$. We point out that for the rest of this section the time index n and the Newton index k are omitted from the $\Delta\mathbf{u}$ and the $\boldsymbol{\lambda}$.

5.2 Active set strategy

The conditions in $(45)_1$ can be identified as the Karush-Kuhn-Tucker conditions of a constrained optimization problem for inequality constraints. To solve this problem we are interested in the correct subset $\mathcal{A}$ of all active vertices of $\mathcal{S}$, for which the body is in contact with the rigid obstacle during a specific time increment Δt. In addition to the subset $\mathcal{A}$, we define with $\mathcal{I}$ all inactive vertices of $\mathcal{S}$, being not in contact within the considered time step. To find the correct subset of active and inactive nodes, we apply the primal-dual active set strategy given in [12]. This approach has been successfully applied to geometrically linear multibody [13] and to materially non-linear [4] contact problems. The active set algorithm within a time increment $[t_n, t_{n+1}]$ will now be summarized. In here the counters k and l represent the corresponding Newton iteration step and the step within the active set loop, respectively.

(0) Initialize $\mathcal{A}_1$ and $\mathcal{I}_1$, such that $\mathcal{S} = \mathcal{A}_1 \cup \mathcal{I}_1$ and $\mathcal{A}_1 \cap \mathcal{I}_1 = \emptyset$ and set $l = 1$.

(1) Find the primal-dual pair $(\Delta\mathbf{u}, \boldsymbol{\lambda})$ by solving the effective structural Equation (36) satisfying

$$\begin{array}{rcll} \Delta u^l_{\nu,i} & = & g^k_{n+1,i} & \text{for all} \quad i \in \mathcal{A}_l, \\ \lambda^l_{\nu,i} & = & 0 & \text{for all} \quad i \in \mathcal{I}_l, \\ \boldsymbol{\lambda}^l_{\tau,i} & = & \mathbf{0} & \text{for all} \quad i \in \mathcal{S}. \end{array} \tag{46}$$

(2) Set $\mathcal{A}_{l+1}$ and $\mathcal{I}_{l+1}$ to

$$\begin{aligned} \mathcal{A}_{l+1} &:= \{i \in \mathcal{S} : \lambda^l_{\nu,i} + (\Delta u^l_{\nu,i} - g^k_{n+1,i}) > 0\}, \\ \mathcal{I}_{l+1} &:= \{i \in \mathcal{S} : \lambda^l_{\nu,i} + (\Delta u^l_{\nu,i} - g^k_{n+1,i}) \leq 0\}. \end{aligned} \tag{47}$$

(3) If $\mathcal{A}_{l+1} = \mathcal{A}_l$ and $\mathcal{I}_{l+1} = \mathcal{I}_l$, then stop, else set $l := l + 1$ and go to step (1).

For further information on this strategy and how to optimize it, e.g. how to handle both iterations in one loop, we refer to the work done by Hüeber and Wohlmuth [13] and Brunssen et al. [4]. We will now derive the final algebraic representation of Equation (46) to be solved in each iteration step. Therefore the diagonal matrix $\mathbf{D}$ is decomposed into

$$\mathbf{D} = \begin{bmatrix} \mathbf{D}_{\mathcal{I}_l} & \mathbf{0} \\ \mathbf{0} & \mathbf{D}_{\mathcal{A}_l} \end{bmatrix}. \tag{48}$$

The normal and the tangential vectors of all active vertices are merged in the matrices $\mathbf{N}_{\mathcal{A}_l}$ and $\mathbf{T}^{(m)}_{\mathcal{A}_l}$ given as:

$$\mathbf{N}^{(|\mathcal{A}_l|\times 3|\mathcal{A}_l|)}_{\mathcal{A}_l} = \begin{bmatrix} \ddots & \ddots & \ddots & 0 & 0 & 0 & 0 & 0 & 0 \\ 0 & 0 & 0 & w_{ii}\nu_{i,x} & w_{ii}\nu_{i,y} & w_{ii}\nu_{i,z} & 0 & 0 & 0 \\ 0 & 0 & 0 & 0 & 0 & 0 & \ddots & \ddots & \ddots \end{bmatrix}, \quad i \in \mathcal{A}_l, \tag{49}$$

where w_{ii} is an abbreviation for the non-zero entries of $\mathbf{D}[i,i]$, having the meaning of a weighting factor, and

$$\mathbf{T}^{(m)(|\mathcal{A}_l|\times 3|\mathcal{A}_l|)}_{\mathcal{A}_l} = \begin{bmatrix} \ddots & \ddots & \ddots & 0 & 0 & 0 & 0 & 0 & 0 \\ 0 & 0 & 0 & t^{(m)}_{i,x} & t^{(m)}_{i,y} & t^{(m)}_{i,z} & 0 & 0 & 0 \\ 0 & 0 & 0 & 0 & 0 & 0 & \ddots & \ddots & \ddots \end{bmatrix}, \quad m = \xi, \eta, \quad i \in \mathcal{A}_l. \tag{50}$$

Herein, $\mathbf{t}_i^{(m)}$ are the associated, normalized tangential vectors given as

$$\mathbf{t}_i^{\xi} \perp \boldsymbol{\nu}_i \quad \text{and} \quad \mathbf{t}_i^{\eta} := \mathbf{t}_i^{\xi} \times \boldsymbol{\nu}_i \quad \text{with} \quad ||\boldsymbol{\nu}_i|| = ||\mathbf{t}_i^{\xi}|| = ||\mathbf{t}_i^{\eta}|| = 1. \tag{51}$$

Now the algebraic representation of (46) and (36) is given by

$$\begin{bmatrix} \mathbf{K}_{eff}^{\mathcal{N}\mathcal{N}} & \mathbf{K}_{eff}^{\mathcal{N}\mathcal{I}_l} & \mathbf{K}_{eff}^{\mathcal{N}\mathcal{A}_l} & \mathbf{0} & \mathbf{0} \\ \mathbf{K}_{eff}^{\mathcal{I}_l\mathcal{N}} & \mathbf{K}_{eff}^{\mathcal{I}_l\mathcal{I}_l} & \mathbf{K}_{eff}^{\mathcal{I}_l\mathcal{A}_l} & \mathbf{D}^{\mathcal{I}_l} & \mathbf{0} \\ \mathbf{K}_{eff}^{\mathcal{A}_l\mathcal{N}} & \mathbf{K}_{eff}^{\mathcal{A}_l\mathcal{I}_l} & \mathbf{K}_{eff}^{\mathcal{A}_l\mathcal{A}_l} & \mathbf{0} & \mathbf{D}^{\mathcal{A}_l} \\ \mathbf{0} & \mathbf{0} & \mathbf{0} & \mathbf{Id}_{\mathcal{I}_l} & \mathbf{0} \\ \mathbf{0} & \mathbf{0} & \mathbf{N}_{\mathcal{A}_l} & \mathbf{0} & \mathbf{0} \\ \mathbf{0} & \mathbf{0} & \mathbf{0} & \mathbf{0} & \mathbf{T}_{\mathcal{A}_l} \end{bmatrix} \begin{bmatrix} \Delta\mathbf{u}_{\mathcal{N}}^l \\ \Delta\mathbf{u}_{\mathcal{I}_l}^l \\ \Delta\mathbf{u}_{\mathcal{A}_l}^l \\ \boldsymbol{\lambda}_{\mathcal{I}_l}^l \\ \boldsymbol{\lambda}_{\mathcal{A}_l}^l \end{bmatrix} = - \begin{bmatrix} \widehat{\mathbf{G}}_{\mathcal{N}} \\ \widehat{\mathbf{G}}_{\mathcal{I}_l} \\ \widehat{\mathbf{G}}_{\mathcal{A}_l} \\ \mathbf{0} \\ -\mathbf{g}_{\mathcal{A}_l}^k \\ \mathbf{0} \end{bmatrix}, \tag{52}$$

where $\mathbf{g}_{\mathcal{A}_l}^k$ is a vector containing the entries $g_{n+1,i}^k$ associated with the active vertex $i \in \mathcal{A}_l$ and $\mathbf{T}_{\mathcal{A}_l} = \begin{bmatrix} \mathbf{T}_{\mathcal{A}_l}^{\xi}, \mathbf{T}_{\mathcal{A}_l}^{\eta} \end{bmatrix}^{\top}$ is a matrix containing the entries associated with the corresponding tangential vectors. We do not directly solve system (52), because this would lead to a change in the size of the system matrices during the calculation, which implies several drawbacks for the performance of a solver. Due to the dual Lagrange multiplier space, the unknown values of $\boldsymbol{\lambda}$ can be locally eliminated using Equation (36).

$$\boldsymbol{\lambda} = \mathbf{D}^{-1} \left(-\widehat{\mathbf{G}}_{\mathcal{S}} - \mathbf{K}_{eff}^{\mathcal{S}\mathcal{N}} \Delta\mathbf{u}_{\mathcal{N}} - \mathbf{K}_{eff}^{\mathcal{S}\mathcal{S}} \Delta\mathbf{u}_{\mathcal{S}} \right) \tag{53}$$

A static condensation yields the reduced system

$$\begin{bmatrix} \mathbf{K}_{eff}^{\mathcal{N}\mathcal{N}} & \mathbf{K}_{eff}^{\mathcal{N}\mathcal{I}_l} & \mathbf{K}_{eff}^{\mathcal{N}\mathcal{A}_l} \\ \mathbf{K}_{eff}^{\mathcal{I}_l\mathcal{N}} & \mathbf{K}_{eff}^{\mathcal{I}_l\mathcal{I}_l} & \mathbf{K}_{eff}^{\mathcal{I}_l\mathcal{A}_l} \\ \mathbf{0} & \mathbf{0} & \mathbf{N}_{\mathcal{A}_l} \\ \mathbf{T}_{\mathcal{A}_l}\mathbf{K}_{eff}^{\mathcal{A}_l\mathcal{N}} & \mathbf{T}_{\mathcal{A}_l}\mathbf{K}_{eff}^{\mathcal{A}_l\mathcal{I}_l} & \mathbf{T}_{\mathcal{A}_l}\mathbf{K}_{eff}^{\mathcal{A}_l\mathcal{A}_l} \end{bmatrix} \begin{bmatrix} \Delta\mathbf{u}_{\mathcal{N}}^l \\ \Delta\mathbf{u}_{\mathcal{I}_l}^l \\ \Delta\mathbf{u}_{\mathcal{A}_l}^l \end{bmatrix} = - \begin{bmatrix} \widehat{\mathbf{G}}_{\mathcal{N}} \\ \widehat{\mathbf{G}}_{\mathcal{I}_l} \\ -\mathbf{g}_{\mathcal{A}_l}^k \\ \mathbf{T}_{\mathcal{A}_l}\widehat{\mathbf{G}}_{\mathcal{A}_l} \end{bmatrix}, \tag{54}$$

to be solved in each Newton step k within one active set loop l. The size of this system remains constant during the calculation and is determined by the finite-element discretization. Looking at Equation (54), we want to point out that this incremental system of equations to be solved does not demand an explicit linearization of the discretized contact virtual work expression. This is quite remarkable, as many of the lately presented segment-to-segment contact approaches require an awkward linearization for the contact forces. In the present approach, the contact forces are calculated from the displacements in a variationally consistent way in a post processing step. The geometric contact constraint of an active vertice $\mathcal{A}_l$ is directly introduced as a Dirichlet boundary condition in a weak, integral sense. Therefore no user defined parameter, like a penalty parameter, is needed in this approach.

6 SPATIAL DISCRETIZATION BY A FINITE SHELL ELEMENT

The spatial discretization of the deformable body is realized by an eight noded, hexahedral surface oriented finite shell element of the Reissner/Mindlin type. Its formulation is based on the shell element presented by Büchter et al. ([5], [6]). A detailed description and several enhancements to this shell formulation are presented by Bischoff [3].

For the application to contact problems, we modify the original description of the shell geometry. In the original formulation, the kinematics of the non-linear shell element is described via a displacement field of the shell mid-surface plus an extensible shell director field. Having the

finite-element nodes situated in the shell mid-surface, the formulation of contact problems becomes quite complicated, as all the integrals for contact have to be performed over the real surface of the shell body. Thus, contact forces acting on the actual shell surface, have to be transmitted to the degrees of freedom, living in the mid-surface. Although this approach has been successfully applied for a classical node-to-segment contact formulation by Gee [10], we reformulate the geometry description, leading to a surface-oriented shell element. With the finite-element nodes now lying on the shell-surface, we can apply the contact approach without any further modification as for any standard hexahedral solid element.

6.1 Approximation of the shell geometry

All the basic assumptions of the shell kinematic remain unmodified. Hence we will only give a very brief review of some basic equations. For a detailed description, we refer to the references given above.

A material point is given by the position vector of the corresponding material point on the shell mid-surface $\mathbf{r}$, the shell director $\mathbf{a}_3$ and the thickness coordinate $\theta^3 \in [-1, 1]$

$$\mathbf{x} = \mathbf{r} + \theta^3 \mathbf{a}_3 \qquad \text{and} \qquad \overline{\mathbf{x}} = \overline{\mathbf{r}} + \theta^3 \overline{\mathbf{a}}_3 \tag{55}$$

in the reference and current configuration, respectively. The deformation of the shell is described by the displacement vector $\mathbf{v}$ and the difference vector $\mathbf{w}$ as

$$\overline{\mathbf{r}} = \mathbf{r} + \mathbf{v} \qquad \text{and} \qquad \overline{\mathbf{a}}_3 = \mathbf{a}_3 + \mathbf{w}. \tag{56}$$

In the surface description, $\mathbf{v}$ and $\mathbf{w}$ are not used as primal displacement unknowns. Instead the geometric relation between the two formulations shown in Figure 4 is used to reparameterize $(\mathbf{v}, \mathbf{w})$ by the displacements on the top and bottom surface of the shell.

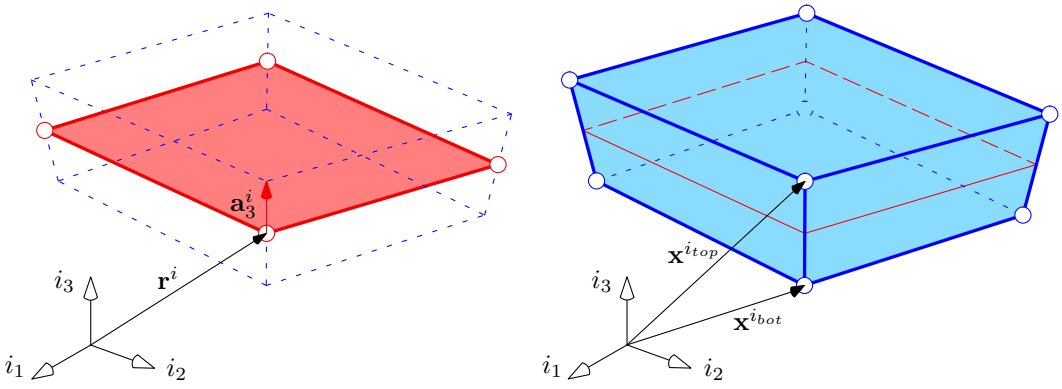

Figure 4: Geometric description of the shell body: left: original - right: modified

Primal displacements $\mathbf{v}^{top}$ and $\mathbf{v}^{bot}$, on the top and bottom surface of the shell element are introduced. Thus the relation between the position vector $\mathbf{r}^i$, the director $\mathbf{a}_3^i$, the displacement vector $\mathbf{v}^i$ and the difference vector $\mathbf{w}^i$ of a specific finite element node in the mid-surface are related to the quantities of the two corresponding shell surface nodes:

$$\begin{aligned} \mathbf{r}^i &= \tfrac{1}{2}\left(\mathbf{x}^{i_{top}} + \mathbf{x}^{i_{bot}}\right), \quad \mathbf{a}_3^i &= \tfrac{1}{2}\left(\mathbf{x}^{i_{top}} - \mathbf{x}^{i_{bot}}\right), \\ \mathbf{v}^i &= \tfrac{1}{2}\left(\mathbf{v}^{i_{top}} + \mathbf{v}^{i_{bot}}\right), \quad \mathbf{w}^i &= \tfrac{1}{2}\left(\mathbf{v}^{i_{top}} - \mathbf{v}^{i_{bot}}\right). \end{aligned} \tag{57}$$

Substituting these relations into the original formulation will end up in slight modifications of the $\mathbf{B}$-operator which connects the displacements to the strains, the geometric stiffness matrix, the mass matrix and the internal force vector. These modifications can be achieved by simply

replacing the discrete element displacement vector of the mid-surface formulation according to the geometric relations given in (57).

$$\begin{aligned} \mathbf{u}^e_{mid} &= (v^1_x\ v^1_y\ v^1_z\ w^1_x\ w^1_y\ w^1_z\ \ldots\ v^4_x\ v^4_y\ v^4_z\ w^4_x\ w^4_y\ w^4_z)^\top \\ &\Downarrow \\ \mathbf{u}^e_{surf} &= (v^{1_{top}}_x\ v^{1_{top}}_y\ v^{1_{top}}_z\ v^{1_{bot}}_x\ v^{1_{bot}}_y\ v^{1_{bot}}_z\ \ldots\ v^{4_{top}}_x\ v^{4_{top}}_y\ v^{4_{top}}_z\ v^{4_{bot}}_x\ v^{4_{bot}}_y\ v^{4_{bot}}_z)^\top \end{aligned} \tag{58}$$

As in the original formulation strain and stress resultants are used within the internal virtual work expression. Also the normal strain enhancement in thickness direction, the so-called 7th parameter, is needed for a consistent solid shell formulation; locking phenomena are treated in the same manner as in the original formulation [3].

6.2 Algorithmic internal forces for GEMM

As already mentioned before, the discretization in time with the Generalized Energy-Momentum Method requires the evaluation of the internal forces at the generalized mid-point configuration. In contrast to the Generalized-α Method, this has a significant influence on the algorithmic evaluation of the internal forces. The starting point is the variation of the Green Lagrange strain tensor at the generalized mid-point configuration and a suitable generalized average of the second Piola Kirchhoff stress tensors at the beginning and the end of a time step. Therefore the internal virtual work is written in terms of these generalized mid-point quantities.

$$\delta\Pi^{int}_{GEMM} = \int_\Omega \delta\mathbf{E}(\mathbf{u}_{n+1-\alpha_f}) : [(1-\alpha_f)\mathbf{S}(\mathbf{u}_{n+1}) + \alpha_f\mathbf{S}(\mathbf{u}_n)]\ d\Omega \tag{59}$$

Within the non-linear shell formulation, the Green Lagrange strain tensor E_{ij} is decomposed into

$$E_{ij} = \alpha_{ij} + \theta^3\ \beta_{ij}, \tag{60}$$

where α_{ij} and β_{ij} represent the constant and linear varying part of $\mathbf{E}$ through the thickness of the shell. The energy conjugent variables to these kinematic variables are the stress resultants, resulting from a thickness integration of the second Piola-Kirchhoff stress tensor.

$$n^{ij} = \int_{-1}^{1} S^{ij}\zeta\ d\theta^3, \qquad m^{ij} = \int_{-1}^{1} \theta^3 S^{ij}\zeta\ d\theta^3 \tag{61}$$

Herein n^{ij} and m^{ij} are the constant and linear parts, respectively, and ζ denotes the shell shifter. According to this formulation, the internal virtual work expression for the Generalized Energy-Momentum Method (59) is given as

$$\delta\Pi^{int}_{GEMM} = \int_M \delta\boldsymbol{\alpha}(\mathbf{u}_{n+1-\alpha_f}) : \mathbf{n}_{n+1-\alpha_f}\ dM + \int_M \delta\boldsymbol{\beta}(\mathbf{u}_{n+1-\alpha_f}) : \mathbf{m}_{n+1-\alpha_f}\ dM, \tag{62}$$

where M denotes the mid-surface of the shell. The stress resultants in the generalized mid-point configuration are defined as

$$\mathbf{n}_{n+1-\alpha_f} = (1-\alpha_f)\mathbf{n}_{n+1} + \alpha_f\mathbf{n}_n \quad \text{and} \quad \mathbf{m}_{n+1-\alpha_f} = (1-\alpha_f)\mathbf{m}_{n+1} + \alpha_f\mathbf{m}_n. \tag{63}$$

Discretization of Equation (62) with the standard isoparametric concept, using bi-linear shape functions to represent the shell mid-surface, will give the algorithmic internal forces for one element.

$$\begin{aligned} \delta\Pi^{e,int}_{GEMM} &\approx \delta\mathbf{u}^e_{surf} \cdot \mathbf{F}^{e,int}(\mathbf{u}_{n+1-\alpha_f}) \\ &= \int_M \delta\mathbf{E}_h(\mathbf{u}_{n+1-\alpha_f}) \cdot \mathbf{S}_h(\mathbf{u}_{n+1-\alpha_f})\ dM \\ &= \delta\mathbf{u}^e_{surf} \int_M \mathbf{B}(\mathbf{u}_{n+1-\alpha_f})^\top \mathbf{S}_h(\mathbf{u}_{n+1-\alpha_f})\ dM \end{aligned} \tag{64}$$

with

$$\mathbf{S}_h = \left[\, n^{11}\ n^{12}\ n^{13}\ n^{22}\ n^{23}\ n^{33}\ m^{11}\ m^{12}\ m^{13}\ m^{22}\ m^{23}\ m^{33} \,\right]^\top \quad \text{and}$$
$$\mathbf{E}_h = \left[\, \alpha_{11}\ \alpha_{12}\ \alpha_{13}\ \alpha_{22}\ \alpha_{23}\ \alpha_{33}\ \beta_{11}\ \beta_{12}\ \beta_{13}\ \beta_{22}\ \beta_{23}\ \beta_{33} \,\right]^\top$$

representing the vectors of the approximated static and kinematic variables, and $\mathbf{B} \in \mathbb{R}^{12\times 24}$ is the differential operator matrix.

6.3 Algorithmic tangent for GEMM

Applying the iterative Newton-Raphson solution scheme, the algorithmic internal forces $\mathbf{F}^{e,int}(\mathbf{u}_{n+1-\alpha_f})$ have to be linearized. In the discretized setting, this will lead to

$$\Delta\delta\Pi^{e,int}_{GEMM} \approx \delta\mathbf{u}_{e,surf} \cdot \mathbf{K}\ \Delta\mathbf{u}_{e,surf} = \delta\mathbf{u}_{e,surf} \cdot [(1-\alpha_f)\mathbf{K}_g + (1-\alpha_f)\mathbf{K}_m]\ \Delta\mathbf{u}_{e,surf} \tag{65}$$

where $\mathbf{K}$ is the algorithmic tangent, which can be split into a material stiffness matrix $\mathbf{K}_m$ and a geometric stiffness matrix $\mathbf{K}_g$ defined as:

$$\mathbf{K}_m = \int_M \mathbf{B}(\mathbf{u}_{n+1-\alpha_f})^\top\ \widehat{\mathbf{C}}\ \mathbf{B}(\mathbf{u}_{n+1})\ dM, \tag{66}$$

$$\mathbf{K}_g = \int_M \mathbf{B}_{,u}^\top\ \mathbf{S}_h(\mathbf{u}_{n+1-\alpha_f})\ dM, \tag{67}$$

where $\widehat{\mathbf{C}} \in \mathbb{R}^{12\times 12}$ is the constitutive matrix obtained after an integration across the thickness. As seen from Equation (66), the material stiffness matrix is non-symmetric, as the differential operators in use, have to be calculated at time $t_{n+1-\alpha_f}$ and t_{n+1}.

For a detailed description for the application of the Generalized Energy-Momentum Method within the context of non-linear shell elements, we will refer to [16].

7 ENERGY CONSERVATION FOR FRICTIONLESS CONTACT

It is known [27, 17, 11] that the application of the presented time integration algorithms, without any special treatment of the contact constraints will not result in an energy conservative method. Dealing with frictionless dynamic contact problems, it is well known that the fulfillment of the so-called *persistency condition*

$$t_\nu(\mathbf{x},t)\dot{g}(\mathbf{x},t) = 0 \tag{68}$$

will lead to an energy conserving scheme. Considering the time continuous case, the *persistency condition* is automatically fulfilled if the Karush-Kuhn-Tucker conditions are satisfied. Various strategies to fulfill this additional constraint (e.g. [18] and [1]) lead to a compromise of violating the geometric admissibility. In this work, we will follow an idea by Laursen and Love [19], introducing a discrete contact velocity $\mathbf{v}^c$ into the algorithmic form of the velocity update.

$$\dot{\mathbf{u}}^{upd}_{n+1} = \dot{\mathbf{u}}_{n+1} + \mathbf{v}^c \tag{69}$$

This additional term is motivated by the fact that the analytical solution of a simple one-dimensional contact problem is characterized by discrete velocity jumps, occurring within one discrete time step. Without an explicit compliance of an algorithmic persistency condition, this strategy allows to treat the geometric contact constraints in an unmodified manner. Thus the impenetrability condition is still satisfied in a weak integral sense. The framework described in Laursen and Love [19] considers the classical midpoint rule. We generalize this approach according to the Generalized-α and the Generalized Energy-Momentum Method, leading to the following form of the velocity update, see Equation (26)

$$\dot{\mathbf{u}}^{upd}_{n+1} = \frac{\gamma}{\beta\Delta t}(\mathbf{u}_{n+1} - \mathbf{u}_n) - \left(\frac{\gamma}{\beta} - 1\right)\dot{\mathbf{u}}_n - \left(\frac{\gamma}{2\beta} - 1\right)\Delta t\ \ddot{\mathbf{u}}_n + \mathbf{v}^c \tag{70}$$

To derive the energy conservation conditions, we follow the procedure described in [19] and perform a special variation of the discretized problem from Equation (27), excluding the damping term and the external forces, since energy conservation does only make sense in this setting. Due to the correction term we solve the dynamic equilibrium

$$\mathbf{M}\left(\ddot{\mathbf{u}}_{n+1-\alpha_m} - \frac{1-\alpha_m}{\gamma\Delta t}\mathbf{v}^c\right) + \mathbf{F}^{int}\left(\mathbf{u}_{n+1-\alpha_f}\right) + \mathbf{F}^c_{n+1-\alpha_f} = \mathbf{0}, \tag{71}$$

and test this equation with (see Equation (70))

$$\Delta\mathbf{u} = \Delta\mathbf{u}^{upd} - \frac{\beta\Delta t}{\gamma}\mathbf{v}^c \tag{72}$$

with

$$\Delta\mathbf{u}^{upd} = \frac{\beta\Delta t}{\gamma}\left[\dot{\mathbf{u}}^{upd}_{n+1} + \left(\frac{\gamma}{\beta} - 1\right)\dot{\mathbf{u}}_n + \left(\frac{\gamma}{2\beta} - 1\right)\Delta t\ \ddot{\mathbf{u}}_n\right]. \tag{73}$$

In the absence of contact, the change in total energy can be expressed as

$$\ddot{\mathbf{u}}^\top_{n+1-\alpha_m}\mathbf{M}\Delta\mathbf{u}^{upd} + \mathbf{F}^{int}\left(\mathbf{u}_{n+1-\alpha_f}\right)^\top\Delta\mathbf{u} = \Delta E^{tot}. \tag{74}$$

In the following, we will only consider all terms arising from the contact forces and the discrete velocity update to arrive at a condition, which satisfies energy-conservation for the contact part. Therefore we test Equation (71) with $\Delta\mathbf{u}$ (Equation (72))

$$0 = (71)\ \Delta\mathbf{u} = \Delta E^{tot} + \Delta E^{num} \tag{75}$$

with the pure numerical gain or loss of energy

$$\Delta E^{num} := \left(-\frac{1-\alpha_m}{\gamma\Delta t}\Delta\mathbf{u}^{upd} + \frac{\beta(1-\alpha_m)}{\gamma^2}\mathbf{v}^c - \frac{\beta\Delta t}{\gamma}\ddot{\mathbf{u}}_{n+1-\alpha_m}\right)^\top\mathbf{M}\mathbf{v}^c + (\mathbf{F}^c_{n+1-\alpha_f})^\top\Delta\mathbf{u}.$$

So the condition

$$\Delta E^{num} = 0 \tag{76}$$

guarantees energy conservation for the contact part. The total energy conservation depends thus on the used time integration scheme. Using the Generalized-α or the Generalized Energy Momentum Method, it is known, that these integration schemes will in general be numerically dissipative. Only in the special case of the midpoint rule, we will exactly conserve the total energy.

After inserting all necessary interpolation definitions into Equation (76) and after quite some algebra, we can express the contact energy-conservation condition in terms of known variables

$$\left(R_1\Delta\mathbf{u} + R_2\dot{\mathbf{u}}_n + R_3\ddot{\mathbf{u}}_n + R_4\mathbf{v}^c\right)^\top\mathbf{M}\ \mathbf{v}^c + (\mathbf{F}^c_{n+1-\alpha_f})^\top\Delta\mathbf{u} = 0. \tag{77}$$

Herein the constants R_i are defined as

$$R_1 = \frac{2(1-\alpha_m)}{\gamma\Delta t}, \quad R_2 = -\frac{(1-\alpha_m)}{\gamma}, \quad R_3 = -\frac{\Delta t}{2\gamma}(2\beta + \alpha_m - 1), \quad R_4 = \frac{\beta(1-\alpha_m)}{\gamma^2}. \tag{78}$$

Let us now define the vector of nodal normal contact forces $\boldsymbol{\lambda}_\nu \in \mathbb{R}^{nc}$ and the matrix

$$\mathbf{N}_n = \begin{bmatrix} \boldsymbol{\nu}_{n,1} & & \\ & \ddots & \\ & & \boldsymbol{\nu}_{n,nc} \end{bmatrix} \in \mathbb{R}^{3nc\times nc}$$

To solve Equation (77) with respect to the unknown discrete velocity jump $\mathbf{v}^c$, we use (see Equation (24) and $(45)_2$)

$$\mathbf{F}^c_{n+1-\alpha_f} = \tilde{\mathbf{D}}\ \mathbf{N}_{n+1-\alpha_f}\ \boldsymbol{\lambda}_\nu \tag{79}$$

to express the contact forces and a similar form

$$\mathbf{M}\mathbf{v}^c = \tilde{\mathbf{D}}\ \mathbf{N}_{n+\alpha_\nu}\ \mathbf{p}_\nu \tag{80}$$

to represent the magnitude of the impulses $\mathbf{p}_\nu$ across the contact surface, presumed to be acting in the direction of a surface normal as well. The parameter $\alpha_\nu \in [0,1]$ provides a sufficiently general description of this impulse in terms of its application at an unspecified configuration $n+\alpha_\nu$. Laursen and Love have shown in ([19]), that $\alpha_\nu = 1$ will preserve angular momentum for a multibody contact problem, thus we will use this value as well. Using Equation (80), we can express the discrete nodal velocity jump as

$$\mathbf{v}^c = \mathbf{M}^{-1}\ \tilde{\mathbf{D}}\ \mathbf{N}_{n+1}\ \mathbf{p}_\nu. \tag{81}$$

Now the expressions (79), (80) and (81) are inserted into Equation (77) to end up with a quadratic expression for the unknown nodal impulse values $\mathbf{p}_\nu$ on Γ_c.

$$\mathbf{p}_\nu^\top \mathbf{A}\mathbf{p}_\nu + \mathbf{b}^\top \mathbf{p}_\nu + c = 0, \tag{82}$$

with

$$\begin{aligned} \mathbf{A} &:= R_4\ \mathbf{N}_{n+1}^\top\ \tilde{\mathbf{D}}^\top\ \mathbf{M}^{-1}\ \tilde{\mathbf{D}}\ \mathbf{N}_{n+1} \\ \mathbf{b} &:= (R_1\ \Delta\mathbf{u} + R_2\ \dot{\mathbf{u}}_n + R_3\ \ddot{\mathbf{u}}_n)^\top\ \tilde{\mathbf{D}}\ \mathbf{N}_{n+1} \\ c &:= \Delta\mathbf{u}^\top\ \tilde{\mathbf{D}}\ \mathbf{N}_{n+1-\alpha_f}\ \boldsymbol{\lambda}_\nu \end{aligned} \tag{83}$$

Of course the quadratic Equation (82) has not a unique solution, as the set of solutions $\mathcal{P}$ is an ellipsoid in $\mathbb{R}^{n_c}$. But, the solution is unique if (82) is fulfilled individually for each nodal point $i \in \Gamma_c$ and Equation (86) given below is satisfied:

$$\sum_{j=1}^{nc} (A^{ij}\ p_{\nu,i}\ p_{\nu,j}) + b^i\ p_{\nu,i} + c^i = 0 \tag{84}$$

A reorganization of this equation will yield a simple quadratic form

$$A^{ii}(p_{\nu,i})^2 + \left[\sum_{j=1, j\neq i}^{nc} A^{ij}\ p_{\nu,j} + b^i\right] p_{\nu,i} + c^i = A^{ii}(p_{\nu,i})^2 + B^i\ p_{\nu,i} + c^i = 0 \tag{85}$$

which can easily be solved, giving two real-valued solutions. Laursen and Love [19] showed that enforcing the condition

$$sign(p_{\nu,i}) = sign(B^i) \tag{86}$$

guarantees that $p_{\nu,i} = 0$ if $\lambda_{\nu,i} = 0$, which is physically meaningful. Once the values of the nodal impulses have been determined, the discrete velocity jump can be calculated using Equation (81), and finally, the update of the velocity field (70) is performed in a post processing step to ensure total energy conservation. For further details of this approach, we refer to the work by Laursen and Love [19]. It must be noted, that in case of impact problems the Lagrange multiplier must be smoothed appropriately in time, since the accelerations and therefore the contact forces are a Dirac impulse which leads to a highly oscillating $\boldsymbol{\lambda}$, see Hauret and Le Tallec [11], where a penalty formulation is used, which shows the problem for high penalty values. So the contact decision (47) has to be modified accordingly.

8 EXAMPLES

Three examples are chosen to examine the performance of the primal-dual active set strategy applied to the described time integration schemes. Various sets of integration parameters are analyzed in view of the evolution of the total energy and the effect of the velocity update. No

physical damping has been assumed. The time integration parameters β, γ, α_m and α_f can be expressed as functions of the spectral radius or of the high frequency dissipation coefficient $\rho_\infty \in [0, 1]$ as

$$\alpha_m := \frac{2\rho_\infty - 1}{\rho_\infty + 1}, \quad \alpha_f := \frac{\rho_\infty}{\rho_\infty + 1}, \quad \beta := \frac{1}{4}(1 - \alpha_m + \alpha_f)^2, \quad \gamma := \frac{1}{2} - \alpha_m + \alpha_f. \tag{87}$$

The choice $\rho_\infty = 1$ corresponds to the case of no algorithmic dissipation, while a smaller $\rho_\infty < 1$ renders dissipation which increases with a decreasing value of ρ_∞.

8.1 Toss rule

To analyze the two different time integration schemes, the different sets of time integration parameters and the effect of the velocity update, we choose the example of the three-dimensional movement of a toss rule. The problem set up, including geometry, material and load time curve is given in Figure 5. For all calculations we use a time step $\Delta t = 50\mu s$. The spatial discretization is done with thirty, eight-noded surface oriented hexahedral shell elements. In Figure 6 the motion of the toss rule is shown, where the calculation is done by the Generalized Energy-Momentum Method with $\rho_\infty = 1.0$. The distribution of the total energy, the kinetic energy and the

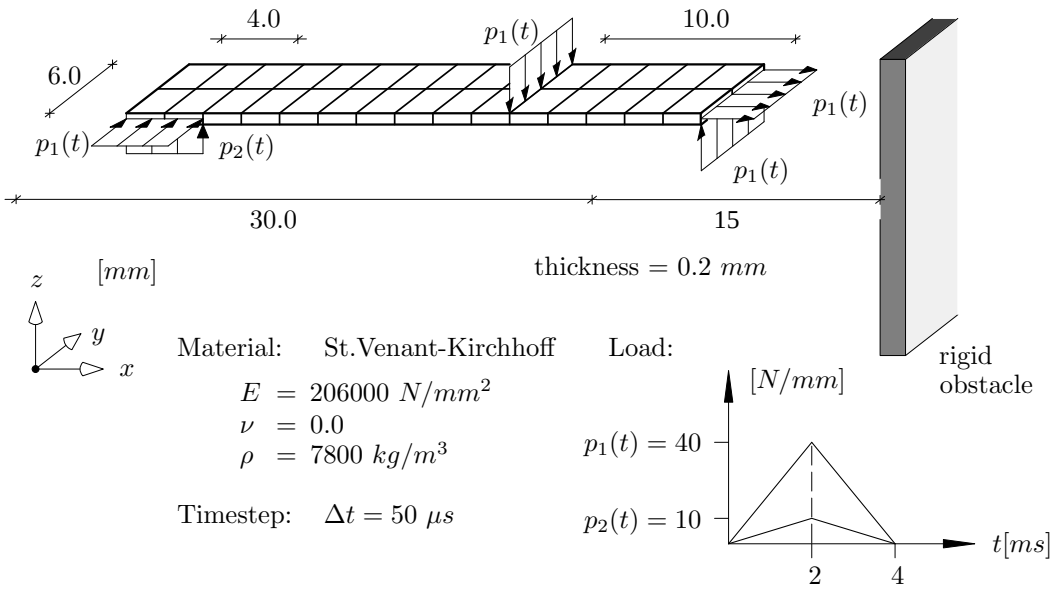

Figure 5: Toss rule - Geometry, Material and Load

strain energy, calculated with the Generalized Energy-Momentum Method and the Generalized-α Method is shown for the case *with* and *without* the velocity update approach in the Figures 7 and 8, respectively. It can be seen that the fully conservation of total energy can only be achieved with the Generalized Energy-Momentum Method, using $\rho_\infty = 1.0$, together with the application of the velocity update algorithm. It is interesting to see that the usage of the velocity update together with the Generalized-α Method does not lead to an improvement concerning the development of the total energy. In case of the General Energy-Momentum Method, the decrease of total energy for a spectral radius $\rho_\infty < 1$ is smoother when the velocity update algorithm is used. We like to point out that the contact algorithm itself turned out to be very robust, regardless of which time integration scheme was used.

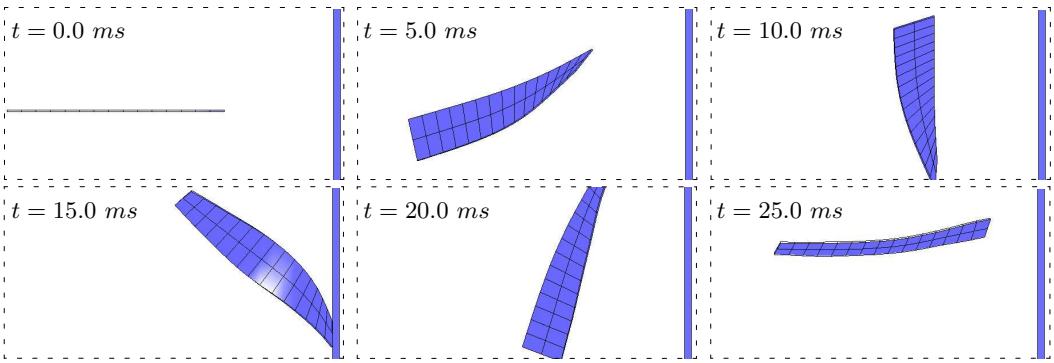

Figure 6: Motion of the toss rule - Generalized Energy-Momentum Method $\rho_\infty = 1.0$

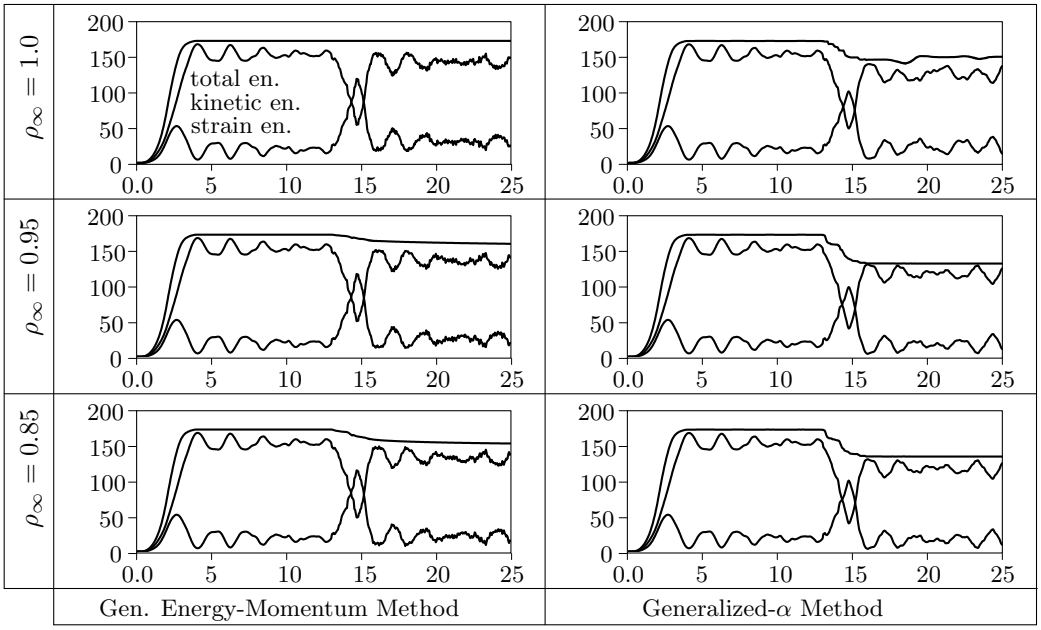

Figure 7: Toss rule - Energy E [J] vs time t [μs] for GEMM and Gen-α *with* velocity update

8.2 Ball

The second example is a thin ball, which is thrown on an inclined rigid obstacle. Geometry, material and position of the applied loads as well as their load time curves are given in Figure 9. A uniform vertical force f_z is applied on the whole outer surface of the ball, whereas the forces in y-direction are applied in positive and negative coordinate axis on one half of the surface of the ball, respectively, which will introduce a slight rotation of the ball.

Following the discussion on the time integration schemes in the first example, we use the Generalized Energy-Momentum Method with $\rho_\infty = 1.0$ for the time discretization. The spatial discretization is done with 256, eight-noded hexahedral surface oriented shell elements. In Figure 10, the motion of the ball is shown for different integration times, as well as the development of the total energy. It can be seen that exact energy conservation can be achieved with the used time integration scheme together with the velocity update algorithm.

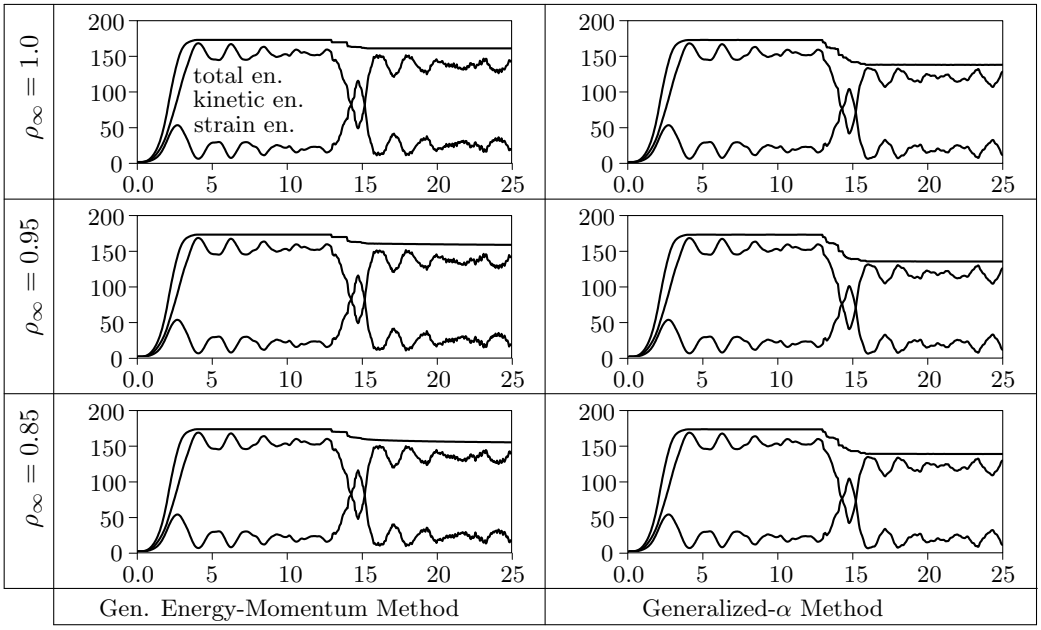

Figure 8: Toss rule - Energy E [J] vs time t [μs] for GEMM and Gen-α *without* velocity update

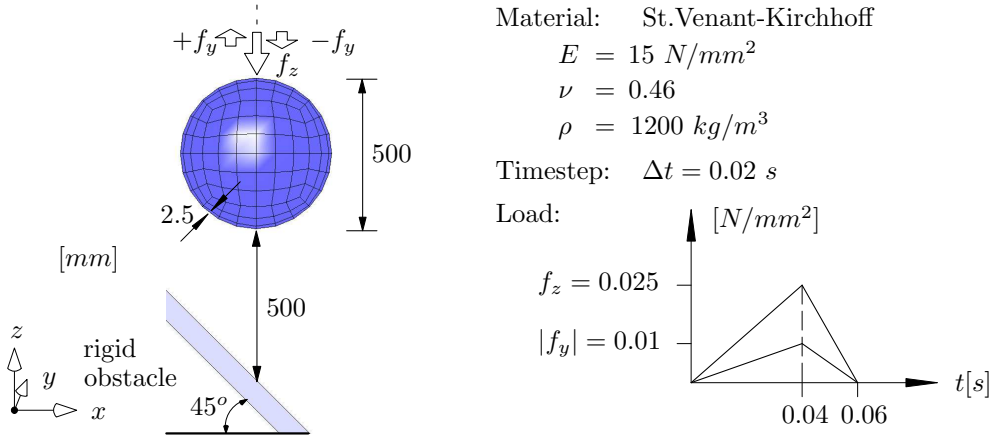

Figure 9: Ball - Geometry, Material and Load

8.3 Torus

With our last example we want to show that the presented contact formulation can be easily extended to frictional contact conditions. We restrict ourselves to a sticking condition, where no tangential sliding is allowed. To show the performance of this approach, we choose a simple rolling contact example, where we suppress sliding in rolling direction $\mathbf{t}^\xi$ only, see Figure 11.

For the implementation the fourth block row of (54) must be split up in a $\mathbf{t}^\xi$-part and a $\mathbf{t}^\eta$-part. The latter remains unchanged, since we still allow tangential sliding orthogonal to the sliding direction, but the $\mathbf{t}^\xi$-part changes to

$$\mathbf{T}_{\mathcal{A}_l} \mathbf{K}_{eff}^{\mathcal{A}_l \mathcal{A}_l} \ \Delta \mathbf{u}_{\mathcal{A}_l}^l = \mathbf{0}.$$

In addition the energy conservation demands to consider now a tangential impulse. We discretize a torus with 384 elements and throw it onto a rigid floor. Geometry, Material and Loads are given in Figure 12, where the load f_r is applied at eight cross-section surfaces, equally distributed

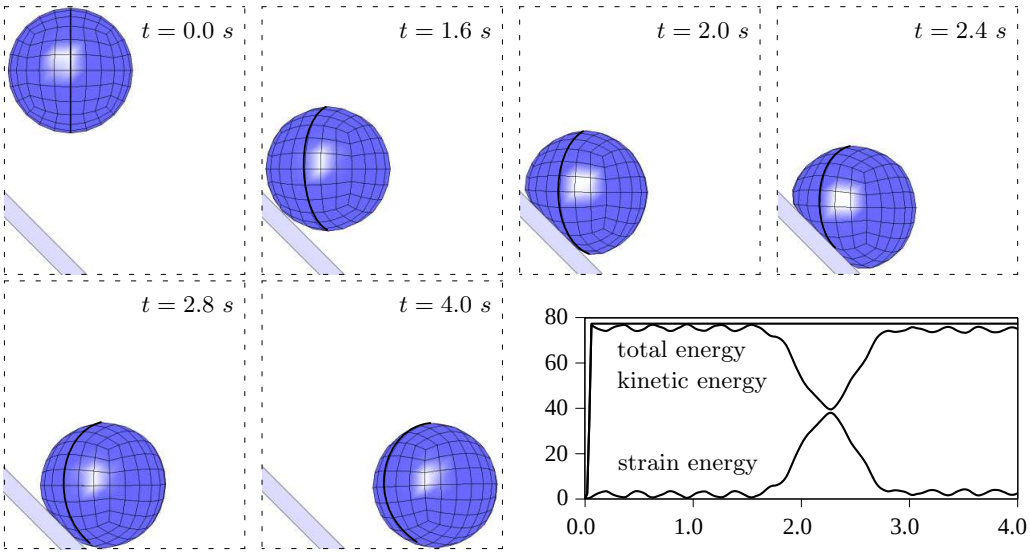

Figure 10: Ball - Motion and Energy E [J] vs time t [s] for GEMM $\rho_\infty = 1.0$

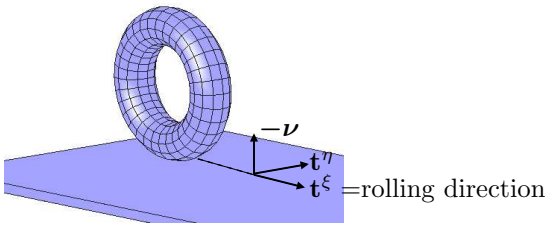

Figure 11: Choice of the normals and tangents for the torus example

around the whole torus, to introduce a slight rotation of the torus. The translatory motion of the torus is initiated by the load f_t, which acts at the inner surface of the torus with an inclined angle of 22.5^o to the rigid obstacle. In Figure 13 the motion of the torus is shown for the case of pure normal contact constrains (no stick condition) and for the modified version with sticking condition in the direction of the motion. To see the different rotations of the toruses we marked one ring of elements with a different color. It is nice to see that in the case of pure normal contact, the torus slides over the rigid obstacle without getting any additional rotational impulse, whereas the example with stick conditions enforces the torus to roll on the surface. Both examples are calculated with the Generalized Energy-Momentum Method with $\rho_\infty = 1.0$. The evolution of the energies are shown in Figure 14. Besides the fact that the total energy is conserved for both cases, it can be seen that the additional stick constraint will shift quite an amount of kinetic energy to the strain energy, due to the larger deformations in this case.

9 CONCLUSIONS

A primal-dual active set strategy based on dual Lagrange multipliers for implicit non-linear analyses of dynamic contact problems is presented. For the time discretization we use the Generalized Energy-Momentum Method and alternatively the Generalized-α Method. The spatial discretization is done by a surface oriented, three-dimensional 7-parameter finite shell element. An energy

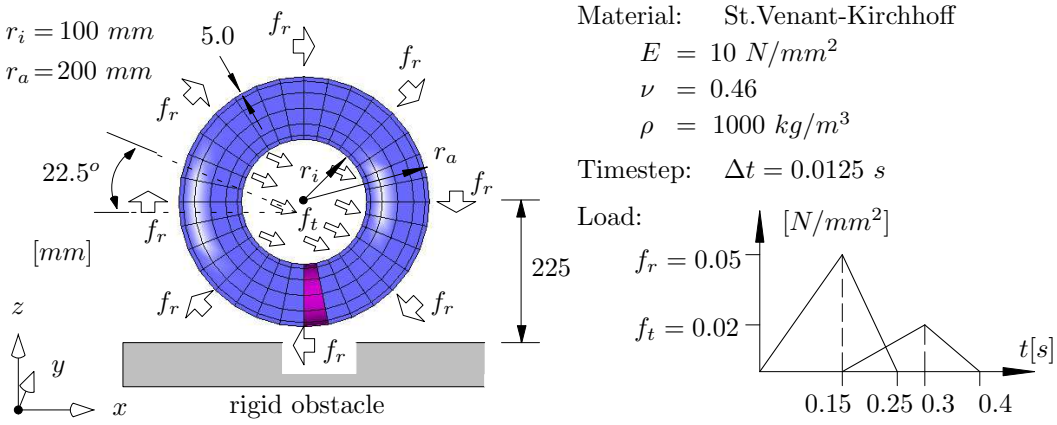

Figure 12: Torus - Geometry, Material and Load

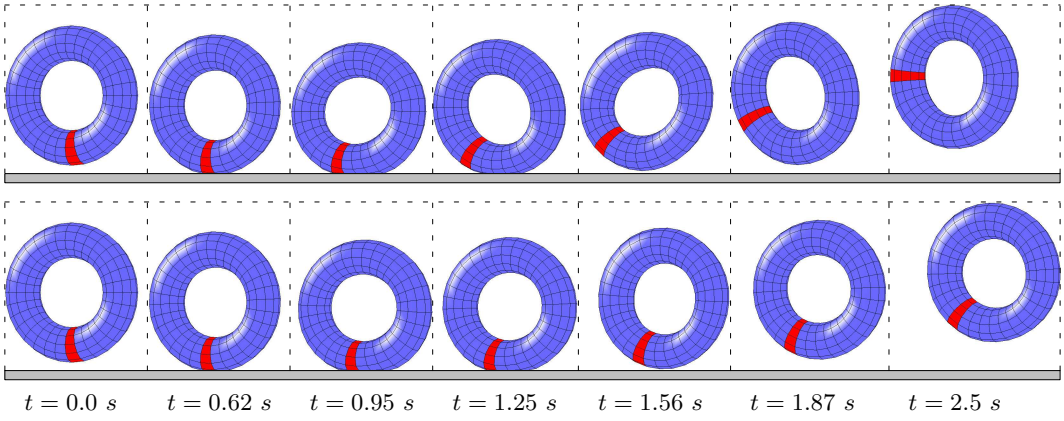

Figure 13: Motion of the torus - Generalized Energy-Momentum Method $\rho_\infty = 1.0$ with (top row) and without stick condition (bottom row)

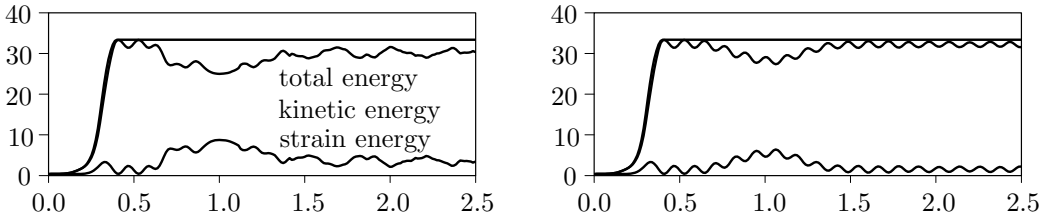

Figure 14: Torus - Energy E [J] vs time t [s] with (left) and without stick condition (right)

conserving framework using a velocity update, introduced by Laursen and Love [19] is generalized to the application within the two mentioned time integration schemes. Furthermore it is adapted to the use of dual Lagrange multipliers for the impulse. The numerical examples show that the proposed strategy leads to a very robust algorithm which can guarantee total energy conservation if the Generalized Energy-Momentum Method is used with a spectral radius $\rho_\infty = 1.0$. In the third example we have shown that this framework can be easily adapted to frictional contact problems.

We like to point out that the presented strategy does not need any user defined parameters such as a penalty parameter to enforce the contact constraints. Furthermore no awkward linearization of the virtual work expression for the contact is involved, which eases the coding effort tremendously

and is therefore much less error-prone.

10 Ackknowledgements

The work in this paper was funded by the German Research Foundation (DFG) through the project WO671/4-1 in the framework of SPP1146: Modeling of incremental forming operations. The authors gratefully acknowledge this support.

References

[1] Armero F, Petocz E. A new class of conserving algorithms for dynamic contact problems. *Computer Methods in Applied Mechanics and Engineering* 1998; **158**:269–300.

[2] Bernardi C, Maday Y, Patera AT. A new nonconforming approach to domain decomposition: the mortar element method. In *Nonlinear partial differential equations and their applications, Collège de France Seminar, XI,* Brezis H, Lions JL (eds). Pitman and Wiley: 1992; 13–51.

[3] Bischoff M. Theorie und Numerik einer dreidimensionalen Schalenformulierung. *Ph.D. Dissertation, Institut für Baustatik, Universität Stuttgart, Bericht-Nr.* **30**, 1999.

[4] Brunssen S, Schmid F, Schäfer M, Wohlmuth B. A fast and robust method for contact problems by combining a primal-dual active set strategy and algebraic multigrid methods. *Preprint 2005/010, Universität Stuttgart* 2005.

[5] Büchter N, Ramm E. 3d-Extension of Nonlinear Shell Equations Based on the Enhanced Assumed Strain Concept. In *Computational Mechanics in Applied Sciences,* C. Hirsch (eds). Elsevier: 1992; 55–62.

[6] Büchter N, Ramm E, Roehl D. Three-dimensional extension of nonlinear shell formulation based on the enhanced assumed strain concept. *International Journal for Numerical Methods in Engineering* 1994; **37**:2551–2568.

[7] Chung J, Hulbert GM. A time integration algorithm for structural dynamics with improved numerical dissipation: The Generalized-α method. *Journal of Applied Mechanics* 1993; **60**:371–375.

[8] Fischer KA, Wriggers P. Frictionless 2D Contact formulations for finite deformations based on the mortar method. *Computational Mechanics* 2005; **36**:226–244.

[9] Flemisch B, Wohlmuth B. Stable Lagrange multipliers for quadrilateral meshes of curved interfaces in 3D *Preprint 2005/005, Universität Stuttgart* 2005.

[10] Gee M. Effiziente Lösungsstrategien in der nichtlinearen Schalenmechanik. *Ph.D. Dissertation, Institut für Baustatik, Universität Stuttgart, Bericht-Nr.* **43**, 2004.

[11] Hauret, P., Le Tallec, P., Energy-controlling time integration methods for nonlinear elastodynamics and low-velocity impact, *Preprint submitted to Elsevier Science*; 2005.

[12] Hintermüller M, Ito K, Kunisch K. The primal-dual active set strategy as a semismooth Newton method. *SIAM J. Optim.* 2003; **13**:865–888.

[13] Hüeber S, Wohlmuth B. A primal-dual active set strategy for non-linear multibody contact problems. *Computer Methods in Applied Mechanics and Engineering* 2005; **194**:3147–3166.

[14] Kikuchi N. and Oden J.T., *Contact problems in elasticity: A study of variational inequalities and finite element methods*, SIAM Studies in Applied Mathematics 8, Philadelphia: 1988.

[15] Kuhl D, Crisfield MA. Energy conserving and decaying algorithms in non-linear structural dynamics. *International Journal for Numerical Methods in Engineering* 1999; **45**:569–599.

[16] Kuhl D, Ramm E. Generalized Energy-Momentum Method for non-linear adaptive shell dynamics. *Computer Methods in Applied Mechanics and Engineering* 1999; **178**:343–366.

[17] Laursen TA. *Computational Contact and Impact Mechanics* Springer: 2002.

[18] Laursen TA, Chawla V. Design of energy conserving algorithms for frictionless dynamic contact problems. *International Journal for Numerical Methods in Engineering* 1997; **40**:863–886.

[19] Laursen TA, Love GR. Improved implicit integrators for transient impact problems - geometric admissibility within the conserving framework. *International Journal for Numerical Methods in Engineering* 2002; **53**:245–274.

[20] McDevitt TW, Laursen TA. A mortar-finite element formulation for frictional contact problems. *International Journal for Numerical Methods in Engineering* 2000; **48**:1525–1547.

[21] Newmark NN. A method of computation for structural dynamics. *Journal of the Engineering Mechanics Division, Proceedings of the American Society of Civil Engineers* 1959; **85**:67–94.

[22] Padmanabhan V, Laursen TA. Surface smoothing procedure for large deformation contact analysis. *Finite Elements in Analysis and Design* 2001; **37**:173–198.

[23] Papadopoulos P, Taylor RL. A mixed formulation for the finite element solution of contact problems. *Computer Methods in Applied Mechanics and Engineering* 1992; **94**:373–389.

[24] Puso MA, Laursen TA. A 3D contact smoothing method using Gregory patches. *International Journal for Numerical Methods in Engineering* 2002; **54**:1161–1194.

[25] Puso MA, Laursen TA. A mortar segment-to-segment contact method for large deformations. *Computer Methods in Applied Mechanics and Engineering* 2004; **193**:601–629.

[26] Puso MA, Laursen TA. A mortar segment-to-segment frictional contact method for large deformations. *Computer Methods in Applied Mechanics and Engineering* 2004; **193**:4891–4913.

[27] Simo J., Laursen T., Augmented lagrangian treatment of contact problems involving friction, *Comput. Struct.* 1992; **42**:97–116

[28] Stadler M, Holzapfel GA. Subdivision schemes for smooth contact surfaces of arbitrary mesh topology in 3D. *International Journal for Numerical Methods in Engineering* 2004; **60**:1161–1195.

[29] Wohlmuth B. A mortar finite element method using dual spaces for the Lagrange multiplier. *SIAM J. Numer. Anal.* 2000; **38**:989–1012.

[30] Yang B, Laursen TA, Meng X. Two dimensional mortar contact methods for large deformation frictional sliding. *International Journal for Numerical Methods in Engineering* 2005; **62**:1183–1225.

Erschienene Preprints ab Nummer 2006/001

Komplette Liste: `http://preprints.ians.uni-stuttgart.de`

2006/001 *Klimke, A.:* Sparse Grid Interpolation Toolbox - User's Guide

2006/002 *Klimke, A., Wohlmuth, B.:* Constructing Dimension-Adaptive Sparse Grid Interpolants using Parallel Function Evaluations

2006/003 *Hartmann, S., Brunssen, S., Ramm, E., Wohlmuth, B.:* Application of a primal-dual active set strategy for unilateral non-linear dynamic contact problems of thin-walled structures